

# Fixed points of the SRG evolution and the on-shell limit of the nuclear force

E. Ruiz Arriola<sup>a</sup>, S. Szpigel<sup>b</sup>, V. S. Timóteo<sup>1c</sup>

<sup>a</sup>*Departamento de Física Atómica, Molecular y Nuclear and Instituto Carlos I de Física Teórica y Computacional  
Universidad de Granada, E-18071 Granada, Spain*

<sup>b</sup>*Centro de Rádio-Astronomia e Astrofísica Mackenzie, Escola de Engenharia, Universidade Presbiteriana Mackenzie  
01302-907, São Paulo, SP, Brasil*

<sup>c</sup>*Grupo de Óptica e Modelagem Numérica - GOMNI, Faculdade de Tecnologia - FT, Universidade Estadual de Campinas - UNICAMP  
13484-332, Limeira, SP, Brasil*

---

## Abstract

We study the infrared limit of the similarity renormalization group (SRG) using a simple toy model for the nuclear force aiming to investigate the fixed points of the SRG evolution with both the Wilson and the Wegner generators. We show how a fully diagonal interaction at the similarity cutoff  $\lambda \rightarrow 0$  may be obtained from the eigenvalues of the hamiltonian and quantify the diagonalness by means of operator norms. While the fixed points for both generators are equivalent when no bound-states are allowed by the interaction, the differences arising from the presence of the Deuteron bound-state can be disentangled very clearly by analyzing the evolved interactions in the infrared limit  $\lambda \rightarrow 0$  on a finite momentum grid. Another issue we investigate is the location on the diagonal of the hamiltonian in momentum-space where the SRG evolution places the Deuteron bound-state eigenvalue once it reaches the fixed point. This finite momentum grid setup provides an alternative derivation of the celebrated trace identities, as a by product. The different effects due to either the Wilson or the Wegner generators on the binding energies of  $A = 2, 3, 4$  systems are investigated and related to the occurrence of a Tjon-line which emerges as the minimum of an avoided crossing between  $E_\alpha = 4E_t - 3E_d$  and  $E_\alpha = 2E_t$ . All infrared features of the flow equations are illustrated using the toy model for the two-nucleon  $S$ -waves.

---

## 1. Introduction

The similarity renormalization group (SRG) approach was proposed independently by Glazek and Wilson and Wegner [1–4] and was initially applied in solid-state physics to simplify many-particle randomly disordered systems. Since the solution of a many-particle problem requires diagonalization of the hamiltonian, a transformation which makes it more diagonal would be of great applicability, specially if the eigenvalues are preserved. This idea was then applied by Wegner in order to suppress the off-diagonal matrix-elements of the hamiltonian by means of unitary transformations [3]. The unitarity of the transformations ensures isospectrality and the generator of the transformations can be chosen to be diagonal if one wants to drive the original hamiltonian towards a band-diagonal form and to suppress its off-diagonal matrix-elements. As a by-product one gets a framework where these off-diagonal components may be better handled in perturbation theory.

The application of the SRG approach to nuclear physics was proposed by Bogner, Furnstahl and Perry [5] with these simplifications in mind and will be our concern here (for reviews see e.g. [6–8] and references therein). The first applications of the SRG method considered high-precision [9, 10] and chiral effective field theory (ChEFT) [11, 12] nucleon-nucleon ( $NN$ ) interactions as the input for the two-body flow equations. Despite different degrees of freedom and types of interaction, the nuclear many-body problem has the same difficulty as the many-electron problem in solid-state physics. More diagonal hamiltonians result in great simplification and faster convergence in nuclear structure calculations. This feature gave rise to a whole program of application of the SRG methods in nuclear physics [5–8]. The formalism was then extended to three-body forces in several schemes [13–15].

---

<sup>1</sup>Corresponding author, tel.: +55 11 981 483 747, e-mail address: varese@ft.unicamp.br

Yet in the two-nucleon system, the interplay between the SRG and a subtractive renormalization approach [16–19] was investigated using the ChEFT  $NN$  interaction at leading-order [20]. Also, the role of long-distance symmetries in effective interactions obtained via SRG flow equations have been recently investigated by us, showing that there is a particular SRG scale at which the  $SU(4)$  spin-isospin Wigner symmetry is realized almost exactly [21, 22]. This is a remarkable result which shows that despite the increasing popularity of the SRG ideas, techniques and extensive computational applications there is still much to be learned from dedicated analysis. The present paper provides further insights along these lines.

The aim of this work is to explore the details underlying our recent results scanning all values of the SRG cut-off and to extend them. In our previous letter [23] a connection between the infrared limit of the SRG evolution with the Wegner generator and Levinson’s theorem [24] was established. Consequences of the infrared interactions for few-nucleon systems and the nuclear many-body problem were discussed in Ref. [25] where a theoretical and phenomenologically successful prediction for the Tjon-line has been advanced. This is a well known existing linear correlation between the binding energies of the triton and the  $\alpha$ -particle which should be expected on the basis of scale invariance [26] (see e.g. [27] for a review and references therein). Further consequences regarding unitary neutron matter in the on-shell limit with a calculation of the Bertsch parameter were addressed in [28] and an SRG discussion of the BCS pairing gap has also been undertaken in Ref. [29].

In this work we investigate the fixed points of the SRG evolution in detail using a simple toy model for the nuclear force in the two-nucleon  $S$ -waves as a particular illustration which simplifies the computational effort considerably and allows for detailed numerical studies in the infrared limit. However, in the infrared region we will suggest that many features are fairly general and model independent. Here we focus on the Wilson and the Wegner SRG generators, since the evolution with a block-diagonal generator [30] in the infrared region has already been studied in previous works [31, 32], where the explicit renormalization of a simple  $NN$  force and the implicit renormalization of a pionless effective field theory (EFT) at next-to-leading order were shown to be equivalent over a wide range of the renormalization scale. The SRG equations are mostly solved numerically on a finite momentum grid with sufficiently many points as to approach the continuum and therefore the grid is viewed as an auxiliary means. Here, we will analyze many effects which can only be clearly disentangled with the aid of this momentum grid, which by itself has some implications on its own and provides both an infrared and ultraviolet cutoffs featuring two basic properties of finite nuclei, namely, the long wavelength character of weak binding systems as well as the finite size of atomic nuclei. Kukulín and collaborators in a series of recent and remarkable works have profited from these finite grids in the few-body problem including both bound and scattering states by analyzing Hamiltonian eigenvalues [33–36]. It is conceivable that a judicious combination of SRG and this approach may provide useful insights into the nuclear few-body problem.

This paper is organized as follows. In Section 2 we present the SRG flow equations in operator form and introduce some useful functional notation both in the continuum limit and in the discretized form which allows for a discussion of fixed points and their stability. In Section 3 we review the toy model which provides a quite reasonable description of the  $NN$  system in the  $S$ -wave channels at low-momenta and will be used in practice to carry out our infrared analysis. In Section 4 we deal specifically with the SRG flow equations on a finite momentum grid. The scattering problem as a Lippmann-Schwinger (LS) equation on the finite momentum grid is analyzed in Section 5. There we provide a motivation to define the phase-shift as an energy-shift which, unlike the conventional phase-shifts determined from the solution of the LS equation, is invariant under unitary transformations on the grid. We illustrate the usefulness of the analysis by re-deriving a set of generalized trace identities, first unveiled by Graham, Jaffe, Quandt and Weigel in Ref. [37], but starting from a momentum grid. Our numerical results on these issues are presented in Section 6. There we focus on the crucial issue of the ordering of states along the SRG evolution trajectory and the remarkable connection to Levinson’s theorem through an energy-shift formula. Our interpretation corrects the erroneous implementation of Kukulín and collaborators [33]. Some of the consequences of the correct identification and ordering of states for the nuclear binding energies when approaching the infrared limit in the  $A = 2, 3, 4$  systems are discussed in Section 7. There the SRG cutoff parameters triggers the avoided crossing pattern, familiar from molecular physics, underlying the Tjon-line correlation. Finally, in Section 8 we present a summary of the results and our main conclusions.

## 2. SRG flow equations in operator form

The similarity renormalization group (SRG) approach, developed by Glazek and Wilson [1, 2] and independently by Wegner [3], has been intensively applied in the context of nuclear physics to handle multi-nucleon forces in order to soften the short-distance core [5, 8] with a rather universal pattern for nuclear symmetries [21, 38] and interactions [39]. The basic strategy underlying the application of the SRG methods to nuclear forces is to evolve an initial (bare) interaction  $H$ , which has been fitted to  $NN$  scattering data, via a continuous unitary transformation that runs a cutoff  $\lambda$  on energy differences. Such a transformation generates a family of unitarily equivalent smooth interactions  $H_\lambda = U_\lambda H U_\lambda^\dagger$  with a band-diagonal structure of a prescribed width roughly given by the SRG cutoff  $\lambda$ .

We employ the formulation for the SRG developed by Wegner [3], which is based on a non-perturbative flow equation that governs the unitary evolution of the hamiltonian with a flow parameter  $s$  that ranges from 0 to  $\infty$ ,

$$H_s = U_s H_0 U_s^\dagger, \quad (1)$$

where  $H_0 \equiv H_{s=0}$  is the initial hamiltonian in the center-of-mass system (CM) and  $U_s$  is the unitary transformation. The flow parameter  $s$  has dimensions of  $[\text{energy}]^{-2}$  and in terms of the SRG cutoff  $\lambda$  with dimension of momentum is given by the relation  $s = \lambda^{-4}$ . As usual, we split the hamiltonian as  $H_s = T + V_s$ , where  $T \equiv T^{\text{cm}} + T^{\text{rel}}$  is the kinetic energy, which we assume to be independent of  $s$ , and  $V_s$  is the evolved potential. For a translational invariant system, i.e.  $V_s \equiv V_s^{\text{rel}}$ , we can separate the CM and consider only the SRG evolution of the hamiltonian for the relative motion,  $H_s^{\text{rel}} = T^{\text{rel}} + V_s^{\text{rel}}$ , since the CM kinetic energy  $T^{\text{cm}}$  does not contribute [40]. For simplicity, in what follows we will drop the superscript “rel”. The SRG flow equation in operator form can then be written as

$$\frac{dH_s}{ds} = \frac{dV_s}{ds} = [\eta_s, H_s], \quad (2)$$

with

$$\eta_s = \frac{dU_s}{ds} U_s^\dagger = -\eta_s^\dagger, \quad (3)$$

and is to be solved with the boundary condition  $H_s|_{s \rightarrow 0} \equiv H_0 = T + V_0$ . The anti-hermitian operator  $\eta_s$  which specifies the unitary transformation  $U_s$  is usually taken as  $\eta_s = [G_s, H_s]$ , where  $G_s$  is a hermitian operator which we will call the SRG generator since it defines  $\eta_s$  and so the flow of the hamiltonian. The most popular choices for the generator are the relative kinetic energy  $G_s = T$  (Wilson generator) [5], the evolving diagonal part of the hamiltonian  $G_s = \text{diag}(H_s) = H_s^D$  (Wegner generator) [2] and the so called block-diagonal generator  $G_s = H_s^{BD} = P H_s P + Q H_s Q$ , where the operators  $P$  and  $Q = 1 - P$  are orthogonal projectors ( $P^2 = P$ ,  $Q^2 = Q$ ,  $QP = PQ = 0$ ) for states below and above a given momentum scale  $\Lambda_{BD}$  [30]<sup>2</sup>.

So far the SRG equations are quite general and can be used to evolve any hamiltonian. In what follows we will restrict to the case of  $NN$  interactions in the center-of-mass (CM) system.

### 2.1. Partial-wave equations

After decomposition of the  $NN$  interaction in partial waves the structure of the SRG flow equations simplifies considerably in the off-diagonal relative momentum-space basis (see e.g. [44] for an explicit derivation and details) for which the following normalization in the completeness relation will be assumed (here and in what follows we use units such that  $\hbar = c = M = 1$ , where  $M$  is the nucleon mass):

$$\frac{2}{\pi} \int p^2 dp |p\rangle \langle p| = \mathbf{1}. \quad (4)$$

Inserting this into Eq. (2) with the Wilson generator,  $G_s = T$ , the flow equation for the SRG evolution of the  $NN$  potential is given by (we drop the partial-wave quantum numbers for simplicity)

$$\frac{dV_s(p, p')}{ds} = -(\epsilon_p - \epsilon_{p'})^2 V_s(p, p') + \frac{2}{\pi} \int_0^\infty dq q^2 (\epsilon_p + \epsilon_{p'} - 2\epsilon_q) V_s(p, q) V_s(q, p'), \quad (5)$$

<sup>2</sup>This is a unitary implementation to all energies of the previously proposed  $V_{\text{lowk}}$  approach [41]. Novel generators have been proposed in [42, 43].

where  $\epsilon_p = \langle p|T|p \rangle = p^2$ . The flow equation for the SRG evolution with the Wegner generator,  $G_s = H_s^D$ , reads

$$\frac{dV_s(p, p')}{ds} = -(\epsilon_p - \epsilon_{p'}) [e_p(s) - e_{p'}(s)] V_s(p, p') + \frac{2}{\pi} \int_0^\infty dq q^2 [e_p(s) + e_{p'}(s) - 2e_q(s)] V_s(p, q) V_s(q, p'), \quad (6)$$

where  $e_p(s) = \langle p|H_s^D|p \rangle = p^2 + V_s(p, p)$ . As we see, these are integro-differential equations which cannot generally be solved analytically (see however [45, 46]) and require a massive computational effort to be solved numerically. We will tackle this problem below by the traditional discretization method of the continuum<sup>3</sup>.

## 2.2. Operator space

Most compact features of the SRG formalism can be best appreciated within an operator space setup. We start with some remarks from the operator theory for finite-dimensional operators in order to introduce some notation (see e.g. the standard textbook [47]). For operators acting on a Hilbert space endowed with a scalar product of states  $\psi$  and  $\varphi$  such as  $\langle \psi, \varphi \rangle$ , we can also define a further scalar product between operators  $A$  and  $B$ , namely

$$\langle A, B \rangle = \text{Tr} [A^\dagger B]. \quad (7)$$

From here we define the Frobenius norm as usual

$$\|A\|^2 = \langle A, A \rangle = \text{Tr} [A^\dagger A], \quad (8)$$

and hence the induced distance between operators as

$$d[A, B] = \|A - B\|. \quad (9)$$

The norm can also be defined as

$$\|A\| = \sup_{\|\psi\|=1} \|A\psi\|, \quad (10)$$

where the standard scalar product induced norm,  $\|\psi\| = \sqrt{\langle \psi, \psi \rangle}$  has been introduced. Of course, this requires finite norm operators  $\|A\| < \infty$  which is unfortunately not the case for the usual unbounded operators in quantum mechanics, such as the kinetic energy. Therefore an ultraviolet cutoff  $\Lambda$  is generally assumed to operate here. Using the partial-wave relative momentum-space normalization metric given in Eq. (4) we have

$$\langle \psi, \psi \rangle = \frac{2}{\pi} \int_0^\infty dp p^2 |\psi(p)|^2. \quad (11)$$

Thus, the kinetic energy would have infinite norm,  $\|T\| \rightarrow \Lambda^2/M \rightarrow \infty$  if everything is taken literally. However, note that the continuum SRG flow equations do not need the kinetic energy to be bound, but rather the potential energy. So, the implicit assumption is that at very high energies the kinetic energy dominates over the potential energy and hence SRG flow equations are well defined provided the value of the potential does not boundlessly grow. The first problems we encounter with all these properties are: i) the fact that the momentum-space basis spans a continuum set and ii) the operators are unbounded. This difficulty is circumvented in practice by using a finite grid in momentum-space and also introducing a high-momentum cutoff  $p_{\text{max}} = \Lambda$  which will be assumed below.

## 2.3. Isospectral flow and fixed points

In this section we briefly review the concepts of isospectral flow and fixed points incorporated in the SRG evolution and the variational interpretation in operator space.

---

<sup>3</sup>However, the usefulness of discretizing the continuum equations goes beyond the practical need of numerically implementing the scattering problem; it provides a theoretical bridge between the energy-shift in the spectrum and the scattering phase-shifts. We will see that this becomes a crucial aspect when the number of grid points is reduced to a minimum.

The isospectrality of the SRG flow equation becomes evident from the trace invariance property of the evolved hamiltonian  $H_s$ . For any choice of the SRG generator  $G_s$  we have a unitary transformation and hence

$$\text{Tr } H_s^n = \text{Tr } H_0^n, \quad (12)$$

for any integer  $n$ . This property follows directly from the commutator structure of the SRG flow equation plus the regulator assumption<sup>4</sup>. Indeed, using the cyclic properties of the trace we get

$$\frac{d}{ds} \text{Tr } H_s^n = n \text{Tr} \left( H_s^{n-1} \frac{dH_s}{ds} \right) = n \text{Tr} \left( H_s^{n-1} [\eta_s, H_s] \right) = 0. \quad (13)$$

Fixed points of the SRG evolution correspond to stationary solutions of the flow equation, Eq. (1),

$$\frac{dH_s}{ds} = [[G_s, H_s], H_s] = 0. \quad (14)$$

This condition implies that there is a basis in which both  $[G_s, H_s]$  and  $H_s$  become simultaneously diagonal at a fixed point. The question is what choices of the generator  $G_s$  actually drive the hamiltonian  $H_s$  to the diagonal form. For generators  $G_s$  which satisfy  $d/\text{Tr } G_s^2 = 0$  and using the cyclic properties of the trace and the invariance of  $\text{Tr } H_s^n$ , we get that

$$\frac{d}{ds} \text{Tr} (H_s - G_s)^2 = 2 \text{Tr} [G_s, H_s]^2 = -2 \text{Tr} \left[ (i [G_s, H_s])^\dagger (i [G_s, H_s]) \right] \leq 0, \quad (15)$$

because  $A \equiv i [G_s, H_s] = A^\dagger$  is a self-adjoint operator and therefore  $A^\dagger A$  is a semi-definite positive operator. Since  $\text{Tr} (H_s - G_s)^2$  is positive but its derivative is negative, the limit  $s \rightarrow \infty$  exists and corresponds to the infrared fixed point of the SRG evolution ( $\lambda \rightarrow 0$ ), at which the hamiltonian  $H_s$  becomes diagonal. Thus, the SRG flow equation just provides a continuous procedure to diagonalize the initial hamiltonian  $H_0 = T + V_0$ .

In the case of the SRG evolution with the Wilson generator,  $G_s = T$ , the flow equation is given by

$$\frac{dH_s}{ds} = \frac{dV_s}{ds} = [[T, H_s], H_s] = [[T, V_s], T + V_s]. \quad (16)$$

We then get for  $\|V_s\| \equiv \text{Tr } V_s^2$  that

$$\frac{d}{ds} \text{Tr } V_s^2 = 2 \text{Tr} [T, V_s]^2 = -2 \text{Tr} \left[ (i [T, V_s])^\dagger (i [T, V_s]) \right] \leq 0. \quad (17)$$

As a consequence of this and using the unitary equivalence,  $H_s = T + V_s = U_s H_0 U_s^\dagger$ , we get that

$$0 < \text{Tr } V_s^2 \leq \text{Tr } V_0^2. \quad (18)$$

Therefore there must be a minimum value obtained at the limit  $s \rightarrow \infty$  which also implies in  $[T, V_{s \rightarrow \infty}] = 0$  due to the stationary condition on the derivative for the infrared fixed point. Hence

$$\lim_{s \rightarrow \infty} \text{Tr } V_s^2 = \min_{V_s} \text{Tr } V_s^2 \Big|_{H_s = T + V_s = U_s H_0 U_s^\dagger}. \quad (19)$$

Thus, in the infrared limit  $s \rightarrow \infty$  ( $\lambda \rightarrow 0$ ) the SRG evolution with the Wilson generator yields asymptotically to the smallest potential, in the Frobenius norm sense, giving the same spectrum as the initial potential  $V_0$  and commuting with the kinetic energy  $T$ , i.e. being diagonal in momentum-space. This is a rather interesting result as it provides a working definition on the “size” of the potential, and moreover different potentials can actually be compared using the distance between the operators induced by the Frobenius norm. Furthermore, this can be interpreted as a quantitative

---

<sup>4</sup>Mathematically, such a property is ill defined in the continuum limit since even for  $n = 1$  one has  $\text{Tr}(V_s) = \int_0^\infty p^2 V_s(p, p) = \int_0^\infty r^2 dr V(r, r)$  which for a local potential  $V(r, r') = V(r)\delta(r - r')$  diverges as the momentum cutoff. Also, the trace of a commutator  $\text{Tr}[A, B]$  only vanishes when both  $\text{Tr}(AB)$  and  $\text{Tr}(BA)$  are finite, as the choice  $A = p$  and  $B = x$  clearly illustrates, since  $[p, x] = -i\hbar$  and hence  $\text{Tr}[p, x] = -i\hbar \text{Tr } \mathbf{1} = \infty$ .

measure of the off-shellness of the interaction. In the partial-wave relative momentum-space basis the orbital degeneracy induced by the  $(2/\pi)p^2 dp$  integration measure in the Frobenius norm has two complementary effects. While it suppresses the contribution to the norm from low-energy states it also enhances the contribution from high-energy components. Thus, minimizing the potential along the SRG evolution trajectory transfers very efficiently high-energy components into low-energy components. This provides a working scheme where any short-distance, or equivalently high-momentum core, becomes softer. It is fair to say that this is the main reason why SRG methods have become popular in realistic nuclear applications. For completeness let us mention that there is an alternative interpretation of softness of the interaction not based on the Frobenius norm, and based on the insightful work of Weinberg [48] and taken up by recent studies from several viewpoints [49, 50] where the repulsive character of the interaction at short-distance plays a key role. At present the connection between these two alternatives, while suggesting different measures of the softness, is somewhat vague and we will not dwell into it here. In our case, we will deal with a potential toy model where the repulsive piece is absent from the start (see Section 3).

In the case of the SRG evolution with the Wegner generator,  $G_s = H_s^D$ , the flow equation is given by

$$\frac{dH_s}{ds} = \frac{dV_s}{ds} = [[H_s^D, H_s], H_s] . \quad (20)$$

Then, in this case we get for  $\|H_s - H_s^D\|^2 \equiv \text{Tr} (H_s - H_s^D)^2$  that

$$\frac{d}{ds} \text{Tr} (H_s - H_s^D)^2 = 2 \text{Tr} [H_s^D, H_s]^2 = -2 \text{Tr} \left[ (i [H_s^D, H_s])^\dagger (i [H_s^D, H_s]) \right] \leq 0 , \quad (21)$$

such that  $\|H_s - H_s^D\| \rightarrow 0$  and so

$$\lim_{s \rightarrow \infty} H_s = H_s^D = \min_{H_s} \|H_s - H_s^D\| , \quad (22)$$

which just shows that the Wegner generator minimizes the distance to its diagonal matrix-elements keeping the eigenvalues of the original Hamiltonian. Of course, if the hamiltonian becomes diagonal the eigenvectors cannot be free momentum eigenstates.

Finally, for the block-diagonal generator we define two orthogonal projection operators  $P + Q = 1$  which split the states below or above a given momentum scale  $\Lambda_{BD}$ . In this case the flow equation is given by

$$\frac{dH_s}{ds} = [[PH_sP + QH_sQ, H_s], H_s] . \quad (23)$$

We then get that the evolution makes the asymptotic hamiltonian block-diagonal hence minimizing the off-diagonal matrix-elements,

$$\lim_{s \rightarrow \infty} H_s = PH_sP + QH_sQ = \min_{H_s} \|H_s - PH_sP - QH_sQ\| . \quad (24)$$

#### 2.4. Discrete equations

Only in few cases the SRG operator equations can be handled in the continuum [45, 46]. In this section we analyze the details of the implementation of the SRG when a finite dimensional reduction of the model space is imposed. The particular case of a momentum grid discretization of the continuum will be discussed specifically in a later section. For simplicity we will consider a basis of eigenstates  $|n\rangle$  of the kinetic energy operator  $T$  on a finite  $N$ -dimensional Hilbert space  $\mathcal{H}_N$ , namely  $T|n\rangle = \epsilon_n|n\rangle$  ( $n = 1, 2, \dots, N$ ), and assume that the corresponding spectrum of eigenvalues  $\epsilon_n$  is non-degenerate (similar to what happens in the partial-wave relative momentum-space basis for which  $\epsilon_n = p_n^2$ ). Thus, the matrix-elements of the hamiltonian  $H = T + V$  in this basis read  $H_{nm} \equiv \langle n|H|m\rangle = \delta_{nm}\epsilon_n + V_{nm}$ .

The discrete SRG flow equations for the matrix-elements of the hamiltonian in the case of the Wilson generator can be written in the form

$$\begin{aligned} \frac{dH_{nm}(s)}{ds} &= \sum_k (\epsilon_n + \epsilon_m - 2\epsilon_k) H_{nk}(s) H_{km}(s) \\ &= -(\epsilon_n - \epsilon_m) [e_n(s) - e_m(s)] H_{nm}(s) + \sum_{k \neq n, m} (\epsilon_n + \epsilon_m - 2\epsilon_k) H_{nk}(s) H_{km}(s) , \end{aligned} \quad (25)$$

where  $H_{nm}(s) = \delta_{nm}\epsilon_n + V_{nm}(s)$  and  $e_n(s) \equiv H_{nn}(s) = \epsilon_n + V_n(s)$ . In the case of the Wegner generator the discrete SRG flow equations read

$$\begin{aligned} \frac{dH_{nm}(s)}{ds} &= \sum_k [e_n(s) + e_m(s) - 2e_k(s)] H_{nk}(s) H_{km}(s) \\ &= -[e_n(s) - e_m(s)]^2 H_{nm}(s) + \sum_{k \neq n, m} [e_n(s) + e_m(s) - 2e_k(s)] H_{nk}(s) H_{km}(s). \end{aligned} \quad (26)$$

These equations are to be solved with the boundary conditions  $H_{nm}(s)|_{s \rightarrow 0} \equiv H_{nm}(0) = \delta_{nm}\epsilon_n + V_{nm}(0)$ .

The fixed points of the SRG evolution with a given generator  $G_s$  correspond to the stationary solutions of the SRG flow equations for the matrix-elements of the hamiltonian,

$$\frac{dH_{nm}(s)}{ds} = \langle n | [[G_s, H_s], H_s] | m \rangle = 0, \quad (27)$$

which implies, for both the Wilson ( $G_s = T$ ) and the Wegner ( $G_s = H_s^D$ ) generators, that in the infrared limit  $s \rightarrow \infty$  ( $\lambda \rightarrow 0$ ) the hamiltonian  $H_s$  becomes diagonal<sup>5</sup>. Thus, we have that

$$\lim_{s \rightarrow \infty} H_{nm}(s) = \delta_{nm} E_n, \quad (28)$$

where  $\{E_n\}_{n=1}^N$  denotes the spectrum of discrete eigenvalues of the hamiltonian  $H_s$  obtained in the infrared limit  $s \rightarrow \infty$ , which are given by

$$E_n \equiv \lim_{s \rightarrow \infty} e_n(s) = \epsilon_n + V_n(s \rightarrow \infty). \quad (29)$$

#### 2.4.1. Ordering of the spectrum induced by the SRG evolution

As we have shown, the SRG evolution with both the Wilson and the Wegner generators on a finite  $N$ -dimensional discrete space have infrared fixed points at which the hamiltonian becomes diagonal. Thus, we have two interpolating SRG trajectories between the initial bare hamiltonian,  $H_0$ , and the final one,  $H_{s \rightarrow \infty}$ . From this point of view, there seems to be no conceptual difference between the SRG evolution with both generators, since the isospectrality of the SRG flow equation guarantees the invariance of the spectrum of eigenvalues of the hamiltonian  $H_s$ . This naive argument overlooks an important detail: the fact that through the SRG evolution the basis of eigenstates  $|\psi_\alpha(s)\rangle$  of the hamiltonian  $H_s$  is actually changing, i.e.

$$U_s |\psi_\alpha(s=0)\rangle = |\psi_\alpha(s)\rangle, \quad (30)$$

and thus the isospectrality does not necessarily fix the final ordering of the eigenvalues which is obtained in the infrared limit  $s \rightarrow \infty$  ( $\lambda \rightarrow 0$ ). This is not a peculiar feature of the SRG evolution; it is shared by *any* diagonalization procedure. In the Gauss elimination method [51], for instance, one makes an arbitrary choice on how to reduce the original matrix to a diagonal form in a finite number of steps; the re-ordering of eigenstates has to be over-imposed at the end by hand, arbitrarily choosing one of the possible permutations of the eigenvalues. Such a re-ordering of eigenstates is equivalent to a unitary transformation. However, unlike the conventional diagonalization methods, the SRG evolution can be interpreted as a *continuum* diagonalization through the flow parameter  $s$ , and thus an infinite number of steps is involved. As a consequence, the SRG evolution induces a very specific ordering of the eigenstates. This, of course, does not provide *exact* results since in practice the infrared limit  $s \rightarrow \infty$  is never

<sup>5</sup>One should note that the stationary condition in operator form, Eq. (14), in principle just requires that at a fixed point both  $[G_s, H_s]$  and  $H_s$  become diagonal in the same basis, not necessarily the one in which the generator  $G_s$  is diagonal. However, we can show that the condition  $[[G_s, H_s], H_s] = 0$  also implies that  $[G_s, H_s] = 0$ . Taking a discrete basis in which  $H_s$  is diagonal, i.e.  $H_{\alpha\beta}(s) = \delta_{\alpha\beta} H_\alpha(s)$ , we have

$$\langle \alpha | [G_s, H_s] | \beta \rangle = \sum_\gamma [G_{\alpha\gamma}(s) H_{\gamma\beta}(s) - H_{\alpha\gamma}(s) G_{\gamma\beta}(s)] = G_{\alpha\beta}(s) [H_\beta(s) - H_\alpha(s)].$$

Thus, for  $\alpha \neq \beta$  we get, in the absence of degeneracies, that  $\langle \alpha | [G_s, H_s] | \beta \rangle = 0$  only if  $G_{\alpha\beta}(s) = 0$  and so both the hamiltonian  $H_s$  and the generator  $G_s$  are diagonal in the same basis. Of course, this becomes a trivial result for generators  $G_s$  which by definition are diagonal in the basis of eigenstates of the kinetic energy operator  $T$ , such as the Wilson and the Wegner generators.

reached, but the errors scale exponentially with the flow parameter  $s$  and are of order  $O[e^{-\min(s, \epsilon_n^2)}]$ . The crucial aspect is that since on a finite dimensional discrete space the SRG flow equation becomes a set of non-linear first-order coupled differential equations for the matrix-elements of the evolved hamiltonian  $H_{nm}(s)$  with the boundary conditions  $H_{nm}(s)|_{s \rightarrow 0} \equiv H_{nm}(0)$ , the uniqueness of the solution implies that just one particular ordering of the eigenvalues takes place asymptotically in the infrared limit  $s \rightarrow \infty$ , which may depend on the choice of the SRG generator  $G_s$ .

Let us consider the initial bare hamiltonian  $H_0$  in the basis of eigenstates  $|n\rangle$  of the kinetic energy operator  $T$  on a finite  $N$ -dimensional Hilbert space  $\mathcal{H}_N$ . The spectrum of eigenvalues  $\{\epsilon_n\}_{n=1}^N$  of the operator  $T$  is assumed to be non-degenerate and arranged in ascending order, i.e.  $\epsilon_1 < \epsilon_2 < \dots < \epsilon_N$ . If we denote by  $\{E_\alpha^0\}_{\alpha=1}^N$  the spectrum of  $N$  discrete eigenvalues of  $H_0$  obtained by any conventional matrix diagonalization method and arranged (by hand) in ascending order similarly to the spectrum of eigenvalues of  $T$ , i.e.  $E_1^0 < E_2^0 < \dots < E_N^0$ , then we have that the final ordering of the spectrum of eigenvalues  $\{E_n\}_{n=1}^N$  of the SRG evolved hamiltonian  $H_s$ , obtained asymptotically in the infrared limit  $s \rightarrow \infty$ , is specifically given by

$$\{E_n\}_{n=1}^N \equiv \{E_{\pi(\alpha)}^0\}_{\alpha=1}^N, \quad (31)$$

where  $\pi(\alpha)$  is one of the  $N!$  possible permutations of the spectrum of  $H_0$ .

It is important to note that in the *continuum* diagonalization of the hamiltonian through the SRG evolution, the correspondence between the kinetic energies  $\epsilon_n$  and the diagonal matrix-elements of the potential  $V_n(s)$  is maintained all the way along the SRG trajectory, as one can clearly see from the expression for the diagonal matrix-elements of the hamiltonian,  $H_{nn}(s) = \epsilon_n + V_n(s)$ . Thus, we have a unique well-defined pairing of the kinetic energies  $\epsilon_n$  with the eigenvalues  $E_n$  obtained asymptotically in the infrared limit  $s \rightarrow \infty$ , namely  $E_n = H_{nn}(s \rightarrow \infty) = \epsilon_n + V_n(s \rightarrow \infty)$ , which is indeed what determines the specific ordering of the spectrum induced by the SRG evolution. One should also note that depending on which particular final ordering of the eigenvalues takes place in the infrared limit  $s \rightarrow \infty$  there may be crossing amongst diagonal matrix-elements of the hamiltonian  $H_{nn}(s)$  along the SRG trajectory. On the other hand, in the conventional diagonalization methods there are  $N!$  different ways of pairing the kinetic energies  $\epsilon_n$  with the eigenvalues  $E_\alpha^0$ , corresponding to the possible orderings of the spectrum. As we have discussed in Ref. [23], this is a crucial issue to establish an isospectral definition of the phase-shift based on an energy-shift approach, which necessarily involves a prescription to order the eigenvalues  $E_\alpha^0$  and set their pairing with the kinetic energies  $\epsilon_n$ .

In section 6 we will illustrate through numerical calculations that when bound-states are allowed by the interaction the phase-shifts evaluated using the energy-shift approach do not comply to Levinson's theorem [24] at low-energies if a naive pairing is set just by ordering the spectrum of eigenvalues  $E_\alpha^0$  in ascending order as the kinetic energies  $\epsilon_n$ ; we further show that the specific ordering of the spectrum induced by the SRG evolution with the Wegner generator in the infrared limit  $s \rightarrow \infty$  remarkably provides a prescription to evaluate the phase-shifts using the energy-shift approach which allows to obtain results that fulfill Levinson's theorem in the presence of bound-states. In section 7 we discuss the inequivalent behaviour of both the Wilson and the Wegner generators in simple variational calculations beyond some critical SRG cutoff approaching the infrared limit.

#### 2.4.2. Stability analysis of the infrared fixed points

As we have pointed out, the uniqueness of the solution of the SRG flow equations on a finite  $N$ -dimensional discrete space implies that a very specific final ordering of the eigenvalues of the hamiltonian is obtained in the infrared limit  $s \rightarrow \infty$  ( $\lambda \rightarrow 0$ ). Of course, the uniqueness of the solution further implies that the infrared fixed point to which the SRG evolved hamiltonian is steadily driven must be asymptotically stable. In this section we will carry out a perturbative stability analysis of the infrared fixed points for both the Wilson and the Wegner generators, which is based on a linearization of the SRG flow equations similar to that described in Ref. [52], as an attempt to determine *a priori* the final ordering of the spectrum induced by the SRG evolution in the infrared limit. As we will see, the perturbative analysis is well-succeeded in predicting the ordering of the spectrum only in the case of the Wilson generator, although the results for both generators are consistent with the analytical proof of diagonalization of the SRG evolved hamiltonian presented in Refs [7, 40].

Let us consider a perturbation of the matrix-elements of the SRG evolved hamiltonian  $H_{nm}(s)$  near an infrared fixed point  $H_{nm}(s \rightarrow \infty) = \delta_{nm}E_n$ , namely

$$H_{nm}(s) = \delta_{nm}E_n + \Delta H_{nm}(s), \quad (32)$$



with the matrix-elements of the perturbation  $\Delta H_{nm}(s)$  required to satisfy the condition  $\Delta H_{nm}(s \rightarrow \infty) = 0$ .

By inserting the perturbed hamiltonian into the SRG flow equation and taking only the terms to first-order in the perturbation we can obtain a set of linearized flow equations for the matrix-elements  $\Delta H_{nm}(s)$ . In the case of the Wilson generator  $G_s = T$ , we get from Eq. (25)

$$\frac{d\Delta H_{nm}(s)}{ds} = -(\epsilon_n - \epsilon_m)(E_n - E_m)\Delta H_{nm}(s). \quad (33)$$

The solutions of these equations for the diagonal matrix-elements ( $n = m$ ) are just constants which actually vanish due to the condition  $\Delta H_{nn}(s \rightarrow \infty) = 0$ , namely  $\Delta H_{nn}(s) \equiv C_{nn} = 0$ , while for the non-diagonal matrix-elements ( $n \neq m$ ) the solutions are given by

$$\Delta H_{nm}(s) = C_{nm}e^{-s(\epsilon_n - \epsilon_m)(E_n - E_m)}, \quad (34)$$

where the integration constants  $C_{nm}$  will depend on the initial conditions set for the matrix-elements  $H_{nm}(s)$  of the perturbed hamiltonian. Thus, we have

$$H_{nm}(s) = E_n\delta_{nm} + C_{nm}e^{-s(\epsilon_n - \epsilon_m)(E_n - E_m)} + \dots \quad (35)$$

Clearly, in the absence of degeneracies the off-diagonal matrix-elements will be ensured to monotonically decrease with  $s$  provided  $(\epsilon_n - \epsilon_m)(E_n - E_m) > 0$ . This implies that from all  $N!$  possible final orderings of the spectrum only the one in which the eigenvalues  $E_n$  are arranged according to the kinetic energies  $\epsilon_n$ , i.e. in ascending order, corresponds to an asymptotically stable infrared fixed point. Thus, in the Wilson generator case the perturbative stability analysis to first-order in the perturbation allows to predict beforehand the specific final ordering of the spectrum induced by the SRG evolution in the infrared limit.

In the case of the Wegner generator  $G_s = H_s^D$ , we get from Eq. (26)

$$\frac{d\Delta H_{nm}(s)}{ds} = -(E_n - E_m)^2\Delta H_{nm}(s). \quad (36)$$

which yields the solution

$$\Delta H_{nm}(s) = C_{nm}e^{-s(E_n - E_m)^2}, \quad (37)$$

such that

$$H_{nm}(s) = E_n\delta_{nm} + C_{nm}e^{-s(E_n - E_m)^2} + \dots \quad (38)$$

As one can see, in this case the off-diagonal matrix-elements will monotonically decrease with  $s$  (in the absence of degeneracies) regardless the ordering of the eigenvalues and so in principle all  $N!$  possible final orderings of the spectrum correspond to asymptotically stable infrared fixed points. Thus, in the Wegner generator case the specific final ordering of the spectrum induced by the SRG evolution in the infrared limit cannot be determined *a priori* through the perturbative stability analysis to first-order in the perturbation and we have to rely on numerical analysis.

### 3. A simple toy model for the $NN$ interaction

We intend to explore the infrared limit of the SRG evolution ( $\lambda \rightarrow 0$ ). Quite generally, the equations to be discussed involve heavy numerical calculations with a discretized continuum spectrum in the case of nuclear physics. The problem is that most of the high-precision potentials, which fit  $NN$  scattering data up to the pion-production threshold ( $\sqrt{m_\pi M_N} \sim 350$  MeV), have a very long tail in momentum space which requires many points and large momentum cutoffs not to miss important contributions. As a consequence the flow equation gets extremely stiff as the SRG cutoff  $\lambda$  approaches zero, such that the computational effort becomes unduly expensive. Actually, there is currently a gap in SRG calculations below  $\lambda \sim 1$  fm<sup>-1</sup> for high-precision [9, 10] and ChEFT [11, 12]  $NN$  potentials.

Therefore, we will illustrate most of our points by using a simple toy model for the  $NN$  interaction which reduces the computational time and allow us to push the SRG evolution towards the infrared limit in a way which is not

practical with realistic interactions. The simplicity of the toy model does not affect the main features of the  $NN$  interaction in the  $S$ -wave channels and gives us the opportunity to investigate the infrared fixed point of the SRG flow equations with any generator. Here we concentrate on the Wilson and the Wegner generators.

Our framework is defined by a toy model for the  $NN$  force in the  $^1S_0$  and the  $^3S_1$  channels which consists of a separable gaussian potential, given by

$$V(p, p') = C g_L(p) g_L(p') = C \exp\left[-(p^2 + p'^2)/L^2\right]. \quad (39)$$

The parameters  $C$  and  $L$  are determined from the solution of the LS equation for the on-shell transition matrix  $T$  by fitting the experimental values of the parameters of the Effective Range Expansion (ERE) to second order in the on-shell momentum, i.e. the scattering length  $a_0$  and the effective range  $r_e$ . Namely, we solve the partial-wave LS equation for the  $T$ -matrix with the toy model potential,

$$T(p, p'; E) = V(p, p') + \frac{2}{\pi} \int_0^\infty dq q^2 \frac{V(p, q)}{E - q^2 + i\epsilon} T(q, p'; E), \quad (40)$$

where  $E$  is the scattering energy, and match the resulting on-shell  $T$ -matrix to the ERE expansion,

$$T^{-1}(k, k; k^2) = -\left[-\frac{1}{a_0} + \frac{1}{2} r_e k^2 + O(k^4) - i k\right] = -[k \cot \delta(k) - i k], \quad (41)$$

where  $k = \sqrt{E}$  is the on-shell momentum in the CM frame and  $\delta(k)$  stands for the phase-shifts. In order to avoid the numerical integration on a contour in the complex plane, we switch to the LS equation for the partial-wave reactance matrix  $K$  with standing-wave boundary conditions,

$$K(p, p'; k^2) = V(p, p') + \frac{2}{\pi} \mathcal{P} \int_0^\infty dq q^2 \frac{V(p, q)}{k^2 - q^2} K(q, p'; k^2), \quad (42)$$

where  $\mathcal{P}$  denotes the Cauchy principal value. The relation between the  $K$ -matrix and the  $T$ -matrix on-shell is given by

$$K^{-1}(k, k; k^2) = T^{-1}(k, k; k^2) - i k = -k \cot \delta(k). \quad (43)$$

Following the method introduced by Steele and Furnstahl [53], we fit the difference between the inverse on-shell  $K$ -matrices corresponding to the toy model potential and the ERE expansion to an interpolating polynomial of degree  $k^2$  for a spread of very small on-shell momenta ( $k \leq 0.1 \text{ fm}^{-1}$ ), namely

$$\Delta K^{-1} = K^{-1}(k, k; k^2) - K_{\text{ERE}}^{-1}(k, k; k^2) = A_0 + A_2 k^2. \quad (44)$$

and then minimize the coefficients  $A_0$  and  $A_2$  with respect to the variations of the parameters  $C$  and  $L$ .

In the case of the separable gaussian potential toy model, given by Eq. (39), it is straightforward to determine the phase-shifts  $\delta(k)$  from the solution of the LS equation for the  $T$ -matrix using the *ansatz*

$$T(p, p'; k^2) = g_L(p) t(k) g_L(p'), \quad (45)$$

where  $t(k)$  is called the reduced on-shell  $T$ -matrix. This leads to the simple relation (valid for separable potentials only)

$$k \cot \delta(k) = -\frac{1}{V(k, k)} \left[ 1 - \frac{2}{\pi} \mathcal{P} \int_0^\infty dq q^2 \frac{1}{k^2 - q^2} V(q, q) \right]. \quad (46)$$

In Table 1 we display the values of the parameters for the toy model potential in the  $^1S_0$  and the  $^3S_1$  channels used in our numerical calculations, which are adjusted to reproduce the corresponding experimental values of  $a_0$  and  $r_e$  by the method described above.

The phase-shifts for the toy model potential in the  $^1S_0$  and the  $^3S_1$  channels evaluated from Eq. (46) are shown in Fig. 1, together with the results obtained from the 1993 Nijmegen partial-wave analysis (PWA) [54] or the more recent 2013 upgrades [55–58]. As one can see, despite the simplicity of the potential and the fact that the  $^3S_1$  channel is not treated as a coupled channel, our toy model for the  $NN$  interaction provides a reasonable qualitative description of the  $S$ -wave phase-shifts. Moreover, the on-shell  $T$ -matrix for the  $^3S_1$  channel toy model potential has a pole located at an imaginary momentum  $k = i\gamma = i 0.2314 \text{ fm}^{-1}$ , corresponding to a satisfactory Deuteron binding-energy  $B_d \simeq 2 \text{ MeV}$ .

Table 1: Parameters for the toy model potential in the  $^1S_0$  and the  $^3S_1$  channels used in the numerical calculations.

-	$a_0$ (fm)	$r_e$ (fm)	$C$ (fm)	$1/L^2$ (fm $^2$ )
$^1S_0$	-23.74	2.77	-1.915884	0.6913
$^3S_1$	5.42	1.75	-2.300641	0.4151

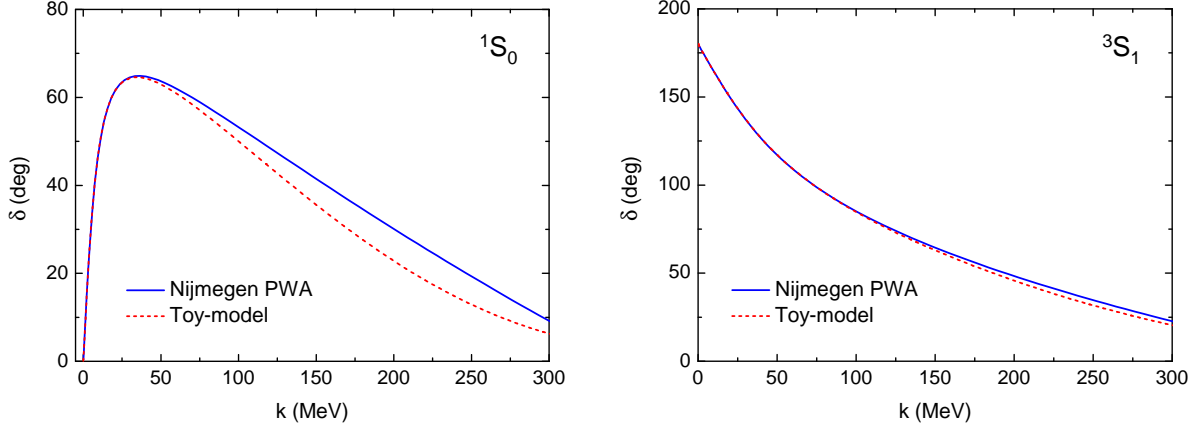


Figure 1: Phase-shifts for the toy model potential in the  $^1S_0$  and the  $^3S_1$  channels compared to the results obtained from the Nijmegen PWA [54].

## 4. SRG on a finite momentum grid

### 4.1. Momentum-space grid

For most cases of interest the SRG flow equations are solved numerically on a finite momentum grid with  $N$  integration points  $p_n$  and weights  $w_n$  ( $n = 1, \dots, N$ ) by implementing a high-momentum ultraviolet (UV) cutoff,  $p_{\max} = \Lambda$ , and an infrared (IR) momentum cutoff,  $p_{\min} = \Delta p$ . The integration rule becomes

$$\int_{\Delta p}^{\Lambda} dp f(p) \rightarrow \sum_{n=1}^N w_n f(p_n). \quad (47)$$

Taking Chebychev-Gauss points [51], for example, we get after re-scaling to the interval  $[0, \Lambda]$ ,

$$p_n = \frac{\Lambda}{2} \left\{ 1 - \cos \left[ \frac{\pi}{N} (n - 1/2) \right] \right\}, \quad w_n = \frac{\Lambda}{2} \frac{\pi}{N} \sin \left[ \frac{\pi}{N} (n - 1/2) \right], \quad (48)$$

and thus

$$p_{\min} = p_1 = \Lambda \sin^2 \left( \frac{\pi}{4N} \right), \quad p_{\max} = p_N = \Lambda \sin^2 \left[ \frac{\pi}{2N} (N - 1/2) \right]. \quad (49)$$

For a large grid and for  $n \ll N$  we have  $p_n = \Lambda(\pi n/2N)^2/2$  which differs from the spherical box quantization. As it is well known, this grid choice guarantees an exact result for polynomials in  $p$  to order  $M \leq N$ , i.e.

$$\int_{\Delta p}^{\Lambda} dp \frac{P_M(p)}{\sqrt{\Lambda^2 - p^2}} = \sum_{n=1}^N w_n \frac{P_M(p_n)}{\sqrt{\Lambda^2 - p_n^2}}. \quad (50)$$

The completeness relation in discretized partial-wave relative momentum-space basis is given by

$$\frac{2}{\pi} \sum_{n=1}^N w_n p_n^2 |p_n\rangle \langle p_n| = \mathbf{1}. \quad (51)$$

Once we have the finite momentum grid we may seek to diagonalize the hamiltonian, whose matrix-elements read

$$H(p_n, p_m) = p_n^2 \delta_{nm} + \frac{2}{\pi} w_n p_n^2 V_{nm} , \quad (52)$$

where  $V_{nm}$  denotes the matrix-elements of the potential  $V(p_n, p_m)$ . The discrete eigenvalue equations on the finite momentum grid are given by

$$p_n^2 \psi_\alpha(p_n) + \frac{2}{\pi} \sum_k w_k p_k^2 V_{nk} \psi_\alpha(p_k) = P_\alpha^2 \psi_\alpha(p_n) , \quad (53)$$

where  $P_\alpha^2$  and  $\psi_\alpha(p_n)$  stand respectively for the eigenvalues and the eigenfunctions of the hamiltonian.

The weight factors  $w_n$  complicate the discrete eigenvalue equations and hide the hermiticity of the hamiltonian. Making a change of variables

$$\psi_\alpha(p_n) = \frac{\varphi_\alpha(p_n)}{p_n \sqrt{2w_n/\pi}} , \quad (54)$$

we have

$$p_n^2 \varphi_\alpha(p_n) + \frac{2}{\pi} \sum_k \sqrt{w_n} p_n V_{nk} \sqrt{w_k} p_k \varphi_\alpha(p_k) = P_\alpha^2 \varphi_\alpha(p_n) . \quad (55)$$

Thus the square-integrability condition reads

$$\frac{2}{\pi} \sum_{n=1}^N w_n p_n^2 |\psi(p_n)|^2 = \sum_{n=1}^N |\varphi(p_n)|^2 , \quad (56)$$

and the multiplication of operators corresponds to the plain matrix multiplication

$$\langle A, B \rangle = \left( \frac{2}{\pi} \right)^2 \int_0^\infty p^2 dp \int_0^\infty k^2 dk A(k, p)^* B(p, k) \rightarrow \left( \frac{2}{\pi} \right)^2 \sum_{n,k=1}^N w_n w_k p_n^2 p_k^2 A_{nk}^* B_{kn} \equiv \sum_{n,k=1}^N \bar{A}_{nk}^* \bar{B}_{kn} , \quad (57)$$

where

$$\bar{A}_{nm} = \frac{2}{\pi} p_n \sqrt{w_n} A_{nm} p_m \sqrt{w_m} . \quad (58)$$

In terms of this new basis the discrete eigenvalue equations become very simple, without the disturbing extra factors, as it was shown in Section 2.4. Note that in the free case,  $V_{nm} = 0$ , we have  $\psi_\alpha(p_n) \sim \delta_{\alpha,n}$ , so that labeling states as distorted states stemming from a given free state,  $p_n \rightarrow P_n$ , means we have an *interacting momentum*. Moreover, in the particular case of a diagonal potential, i.e.  $V_{nm} = \delta_{nm} V_n$ , Eq. (53) yields a relation which resembles a self-energy equation,

$$p_n^2 + \frac{2}{\pi} w_n p_n^2 V_n = P_n^2 , \quad (59)$$

where  $P_n^2$  denotes the eigenvalues of the hamiltonian.

#### 4.2. SRG flow equations

The SRG flow equations on the finite momentum grid for the matrix-elements of the potential in a given partial wave follow from inserting the completeness relation, Eq. (82), into the SRG flow equation in operator form, Eq. (2). In the case of the Wilson generator we get

$$\frac{dV_{nm}(s)}{ds} = -(p_n^2 - p_m^2)^2 V_{nm}(s) + \frac{2}{\pi} \sum_k w_k p_k^2 (p_n^2 + p_m^2 - 2p_k^2) V_{nk}(s) V_{km}(s) , \quad (60)$$

and in the case of the Wegner generator,

$$\frac{dV_{nm}(s)}{ds} = -(p_n^2 - p_m^2) [e_n(s) - e_m(s)] V_{nm}(s) + \frac{2}{\pi} \sum_k w_k p_k^2 [e_n(s) + e_m(s) - 2e_k(s)] V_{nk}(s) V_{km}(s), \quad (61)$$

where  $e_n(s) = p_n^2 + \frac{2}{\pi} w_n p_n^2 V_s(p_n, p_n)$

The eigenvalue problem on the finite momentum grid for the SRG-evolved hamiltonian  $H_\lambda = U_\lambda H U_\lambda^\dagger$  may be formulated as

$$H_\lambda |\alpha, \lambda\rangle = P_\alpha^2 |\alpha, \lambda\rangle, \quad (62)$$

where  $|\alpha, \lambda\rangle$  are the eigenstates of  $H_\lambda$ . The matrix-elements of the hamiltonian  $H_\lambda$  and the corresponding eigenfunctions  $\psi_{\alpha, \lambda}$  in momentum-space representation are given respectively by

$$H_\lambda(p_n, p_m) = p_n^2 \delta_{nm} + \frac{2}{\pi} w_n p_n^2 V_\lambda(p_n, p_m) \quad (63)$$

and

$$\psi_{\alpha, \lambda}(p_n) = \langle n | \alpha, \lambda \rangle. \quad (64)$$

A bound-state with (negative) eigenvalue  $P_\alpha^2 = -B_\alpha$  corresponds to a pole in the scattering amplitude at imaginary momentum  $P_\alpha = i\gamma$ . Because of the commutator structure of the SRG flow equation the isospectrality property still holds on the grid and therefore the eigenvalues  $P_\alpha^2$  of  $H_\lambda$  are  $\lambda$ -independent, i.e.

$$\frac{dP_\alpha}{d\lambda} = 0. \quad (65)$$

As we have discussed in section 2.4, although the isospectrality property ensures that the eigenvalues of the hamiltonian remain invariant along the SRG trajectory, the ordering of the states may depend on the specific choice of the SRG generator  $G_s$ . This yields to an interesting feature observed systematically in SRG calculations when bound-states are allowed by the interaction. In the presence of bound-states (real or spurious), hamiltonians evolved using the Wilson and the Wegner generators begin to flow differently when the SRG cutoff  $\lambda$  approaches some critical momentum  $\Lambda_c$ , which corresponds to the threshold scale where the bound-state emerges [59, 60] (one should note that the critical momentum  $\Lambda_c$  is distinct from the characteristic bound-state momentum scale  $\gamma$ ). This is explicitly verified by a block-diagonal generator analysis [61] (see also an analysis based just on scattering information [23] using Effective Field Theory ideas). In the Wilson generator case the bound-state remains coupled to the low-momentum scales as  $\lambda$  approaches  $\Lambda_c$ , such that the bound-state eigenvalue is pushed towards the lowest momentum available on the grid,  $p_1$ , which corresponds to the IR momentum cutoff  $\Delta p$ . Moreover, matrix-elements of the potential at low-momentum diverge when  $\Delta p \rightarrow 0$  in order to force the bound-state eigenvalue to smaller momenta, such that the SRG evolution may become numerically unstable. In the Wegner generator case the bound-state decouples from the low-momentum scales as  $\lambda$  approaches  $\Lambda_c$ , being placed on the diagonal of the hamiltonian as an isolated negative eigenvalue at a momentum  $p_{n_{BS}}$  between the lowest momentum on the grid  $p_1$  and the critical momentum  $\Lambda_c$ . As pointed out in Ref. [60], the *a priori* determination of the position at which the bound-state is placed on the diagonal when using the Wegner generator is still an open problem. It is important to note that when the SRG cutoff  $\lambda$  is kept well above the critical momentum  $\Lambda_c$  or in the absence of bound-states the SRG evolutions using the Wilson and the Wegner generators are nearly identical, a behavior that can be traced to the dominance of the kinetic energy.

## 5. The scattering problem on a finite momentum grid

So far we have dealt with the evolution of the hamiltonian according to the SRG flow equations, which take a manageable form in the discrete momentum basis. In this section we exploit the same basis to analyze the scattering problem and point out several specific features unveiled in our previous work [23] and extending them.

Of course, the momentum grid should in principle be arbitrary. In the next section we consider a physically motivated procedure based on considering a spherical box which introduces a quantization condition for the momentum

and also allows a straightforward determination of the phase-shifts at the quantized momentum values. However, this finite box scheme makes the choice of the grid to depend on the angular momentum. Afterwards we will consider the standard and fixed gaussian integration grid which is valid for all partial waves, although the identification of the phase-shifts is less obvious.

### 5.1. LS equation and phase-shifts

For the case of nuclear hamiltonians and more specifically for the  $NN$  situation, the scattering problem requires defining phase-shifts. Unfortunately, the standard methods to handle the scattering problem in momentum-space do it through the numerical solution of the LS equation, which introduce a momentum grid but do not allow to compute the phase-shifts on the *same* grid points. In fact there appear two different grids where a difference between the so-called observation points in discrete energy values and the momenta on discrete values are not in one-to-one correspondence. For our purposes, it becomes necessary to use a method where the phase-shifts can be defined on the momentum grid *without* extra observation points.

In operator form, the LS equation for the  $T$ -matrix of a two-body system reads

$$T(E) = V + V G_0^+(E) T(E) , \quad (66)$$

where  $E$  is the scattering energy and  $G_0^+(E) = (E - h_0 + i\epsilon)^{-1}$  is the free Green's function with outgoing-wave boundary conditions given in terms of the free hamiltonian  $h_0$  (which corresponds to the kinetic energy operator  $T$ ).

The LS equation for the  $T$ -matrix on the finite momentum grid is obtained by taking the matrix-elements in the discretized partial-wave relative momentum-space basis and reads

$$T_{nm}(p) = V_{nm} + \frac{2}{\pi} \sum_{k=1}^N w_k \frac{p_k^2}{p^2 - p_k^2 + i\epsilon} V_{nk} T_{km}(p) , \quad (67)$$

where  $p^2$  is the scattering energy  $E$ . Note that the momentum  $p$  corresponding to the observation point can in principle be chosen independently of the momentum grid. The on-shell limit is obtained by taking  $p = p_n$  on the grid. We switch to the  $R$ -matrix, which on the grid yields the LS equation for the half-on-shell amplitude

$$R_{nm}(p_n) = V_{nm} + \frac{2}{\pi} \sum_{k \neq n} w_k \frac{p_k^2}{p_n^2 - p_k^2} V_{nk} R_{km}(p_n) , \quad (68)$$

where the excluded sum embodies the principal value prescription of the continuum version, Eq. (42). This equation can be solved by inversion for any grid point  $p_n$  and thus we obtain the LS phase-shift <sup>6</sup>

$$- \frac{\tan \delta^{\text{LS}}(p_n)}{p_n} = R_{nn}(p_n) . \quad (69)$$

In Fig. 2 we show the phase-shifts for the toy model separable gaussian potential in the  $^1S_0$  and the  $^3S_1$  channels evaluated from the solution of the LS equation on the grid *at the observation grid points* for a high-momentum UV cutoff  $\Lambda = 2 \text{ fm}^{-1}$  and different number of grid points  $N$ , compared to the exact results obtained from the solution of the standard LS equation in the continuum limit ( $N \rightarrow \infty$ ).

### 5.2. Energy-shift in a box: coordinate space

While the momentum grid provides a viable alternative to solve both the SRG and the scattering equations, since it corresponds to a discretization of the integration rule, it is useful to consider a physically motivated situation where this momentum discretization naturally appears. Thus, we analyze the effects of having a large spherical box in

---

<sup>6</sup>The explicit, and apparently pedantic, LS label in  $\delta^{\text{LS}}(p_n)$  is not redundant; it does reflect the dependence on the choice of the LS equation, the grid and the number of grid points. This will become clear below when we show the inequivalence of these phase-shifts on a finite momentum grid along the SRG trajectories.

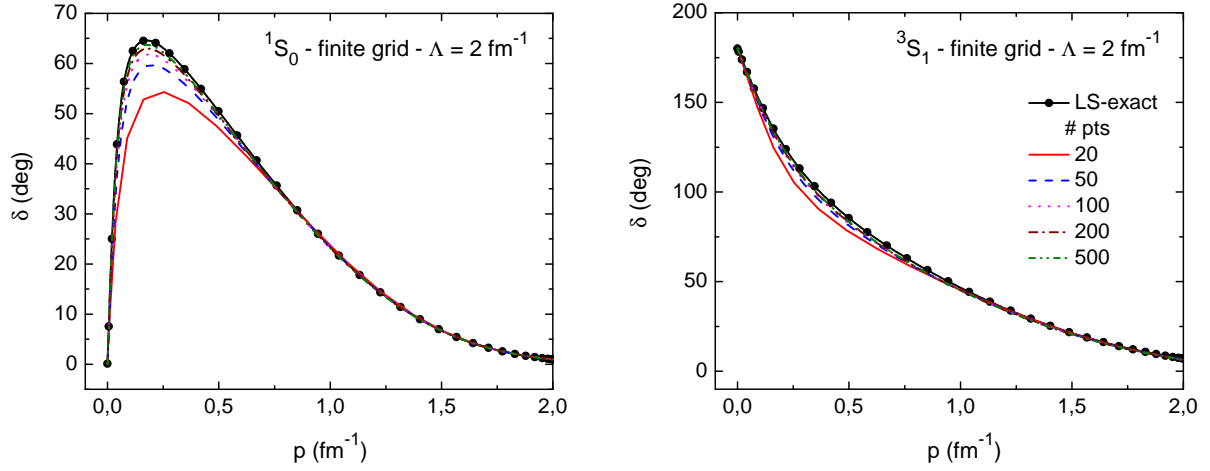


Figure 2: Phase-shifts for the toy model separable gaussian potential in the  $^1S_0$  and the  $^3S_1$  channels evaluated from the solution of the LS equation on the grid *at the grid points* for a high-momentum UV cutoff  $\Lambda = 2 \text{ fm}^{-1}$  and different number of grid points  $N$ . For comparison, we also show the exact phase-shifts obtained from the solution of the standard LS equation in the continuum limit ( $N \rightarrow \infty$ ).

three dimensions for a central potential. The case of a cubic box, which would be relevant for finite volume lattice calculations, has the disadvantage of breaking the symmetries of the problem and will be studied elsewhere.

Let us consider for simplicity a local and finite range potential  $V(r)$  with a range larger than a certain distance  $a$ . For the  $S$ -wave at large distances, i.e. outside of the range of the potential, we have

$$u(r) = \sin[pr + \delta(p)] . \quad (70)$$

If the size of the box  $L$  is larger than the range  $a$  of the potential then the condition of the particle confined to be inside the finite box is

$$u(L) = 0 \rightarrow p_n L + \delta(p_n) = n\pi , \quad (71)$$

which is a quantization condition for the allowed momentum  $p$ . Thus, the effect of the finite box is to discretize the momenta. In the free case we have  $p_{n,0}L = n\pi$ , and then we may write the shift in momentum due to the interaction as follows

$$\Delta p_n = p_n - p_{n,0} = -\frac{1}{L}\delta(p_n) \rightarrow -\frac{1}{L}\delta(p) + O(L^{-2}) , \quad (72)$$

where in the last line we assume a large box and a smooth behavior of the phase-shift. This means that the spectrum gets a distortion which scales inverse proportional to the size of the box. Note that this result is strictly valid for large box sizes. In the case where the box size is not much larger than the range of the potential, but still  $L \gtrsim a$  the quantization condition is actually a non-linear eigenvalue equation.

The interesting thing is that integrals over momentum get discretized and one has

$$\int \frac{dp}{2\pi} f(p) \rightarrow \frac{1}{L} \sum_n f\left(\frac{n\pi}{L}\right) . \quad (73)$$

For instance if we sum over functions of eigenvalues of the hamiltonian

$$\sum_n F(E_n) = \sum_n F(E_n^{(0)}) - \frac{1}{L} \sum_n F'(E_n^{(0)}) \delta(p_{n,0}) , \quad (74)$$

which can be re-written as

$$\text{Tr} F(H) = \text{Tr} F(H_0) - \int \frac{dp}{2\pi} F'(E) \delta(p) . \quad (75)$$

The procedure above can be generalized to all partial waves, since far from the potential we have

$$u_l(r)/r = \sin \delta_l(p) j_l(pr) - \sin \delta_l(p) y_l(pr) , \quad (76)$$

so that the box boundary condition yields

$$\sin \delta_l(p) j_l(pL) - \sin \delta_l(p) y_l(pL) = 0 , \quad (77)$$

and obviously the momenta are quantized but also depend on angular momentum.

### 5.3. From energy-shift to phase-shift

The previous analysis motivated Lifshitz many years ago, when studying the impurities in a crystal lattice, to propose a generalization of the quantization condition based on an arbitrary finite momentum grid. This approach, also pursued independently by DeWitt [62] and Fukuda and Newton [63], has been taken over in nuclear physics for the analysis of the few-body scattering problem by Kukulin and collaborators in a series of recent and remarkable works [33–36]. The basic idea is to solve the scattering problem without solving the scattering equations but just the eigenvalue equations for the discretized hamiltonian in the continuum limit. One should note that while the box quantization condition corresponds to a specific momentum grid choice,  $p_n = n\pi/L$  and  $w_n = \pi/L$  in the free case, a general momentum grid does not have an obvious meaning.

One important feature of the previous form of the LS equation for the  $R$ -matrix on a finite momentum grid, Eq. (68), is that the Cauchy principal value for the integral becomes an excluded summation which is not symmetric since the distance above and below the pole differs, i.e.  $p_{n+1}^2 - p_n^2 \neq p_n^2 - p_{n-1}^2$ . This induces some finite asymmetry which is ultimately pointwise removed in the continuum since it scales as  $w_n$ . However, when summing up the spectrum with weight  $w_n$  the net effect is finite. Thus, if we consider the matrix  $R_{nm}(p)$  as a function of the external momentum  $p = p_n$  on the grid corresponding to the scattering energy  $p_n^2$ , we get trivially from Eq. (68) that  $R_{nm}(p_n) = V_n$  for a diagonal potential  $V_{nm} = \delta_{nm} V_n$ , such that Eq. (59) can be written in the form

$$p_n^2 + \frac{2}{\pi} w_n p_n^2 R_{nm}(p_n) = P_n^2 . \quad (78)$$

A comparison of this relation in the continuum limit,  $w_n \rightarrow 0$ , with the treatment presented in the previous section for the large box quantization in coordinate space suggests the identification

$$R_{nm}(p_n) = \frac{\pi}{2} \frac{(P_n^2 - p_n^2)}{w_n p_n^2} \rightarrow -\frac{\delta^{\text{ES}}(p_n)}{p_n} , \quad (79)$$

which provides an energy-shift formula to define the phase-shift,

$$\delta^{\text{ES}}(p_n) = -\frac{\pi}{2} \frac{(P_n^2 - p_n^2)}{w_n p_n} . \quad (80)$$

Of course, both the energy-shift (ES) and the LS definitions for the phase-shift lead to the same results in the continuum limit,  $w_n \rightarrow 0$ . However, for a finite momentum grid there are important differences which are relevant for the SRG evolution, namely, for unitary transformations on the grid the energy-shift definition of the phase-shift provides invariant results along the SRG trajectory unlike the LS phase-shift (see below). One should also note that the energy-shift formula for the phase-shift is not unique. We could instead use a momentum-shift formula very much in agreement with the finite box treatment. Quite generally, all these possible formulas become equivalent in the continuum limit, but for a finite number  $N$  of grid points we should expect differences. It would be highly interesting to design formulas where improved accuracies for finite  $N$  are displayed. We leave this interesting topic for future research. Finally, it is important to note that for a finite momentum grid with dimension  $N$  there are  $N!$  possible permutations for the eigenvalues  $P_n^2$  obtained from the diagonalization of the hamiltonian and so the evaluation of phase-shifts using the energy-shift approach necessarily involves an ordering prescription.



#### 5.4. Phase-equivalence and inequivalence

As pointed out before the original motivation for the application of the SRG in the context of nuclear physics was to soften the  $NN$  interaction while keeping the phase-shifts invariant. In our previous work [23] we have shown that on a finite momentum grid phase-equivalence does not hold along the SRG trajectory for the LS definition, while for the isospectral definition based on the energy-shift formula phase-equivalence is preserved. In this section we elaborate more on this issue.

First, let us consider the eigenstate decomposition of the LS equation for the  $T$ -matrix on a finite momentum grid with the SRG-evolved potential, which can be written in operator form as

$$T(E) = V_\lambda + V_\lambda(p^2 - H_\lambda + i\epsilon)^{-1} V_\lambda . \quad (81)$$

Taking the matrix-elements in the discretized partial-wave relative momentum-space basis and inserting a complete set of eigenstates of the SRG-evolved hamiltonian  $H_\lambda = U_\lambda H U_\lambda^\dagger$ , namely

$$\sum_\alpha |\alpha, \lambda\rangle \langle \alpha, \lambda| = \mathbf{1} , \quad (82)$$

we obtain

$$T_{nm}(p) = V_{nm}(\lambda) + \left(\frac{2}{\pi}\right)^2 \sum_{k=1}^N \sum_{l=1}^N (w_k p_k^2) (w_l p_l^2) \sum_\alpha V_{nk}(\lambda) \frac{\psi_{\alpha,\lambda}(p_k) \psi_{\alpha,\lambda}(p_l)}{p^2 - P_\alpha^2 + i\epsilon} V_{lm}(\lambda) , \quad (83)$$

Switching to the  $R$ -matrix at the grid points  $p = p_n$ , we get

$$R_{nm}(p_n) = V_{nm}(\lambda) + \left(\frac{2}{\pi}\right)^2 \sum_{k \neq n} \sum_l (w_k p_k^2) (w_l p_l^2) \sum_\alpha V_{nk}(\lambda) \frac{\psi_{\alpha,\lambda}(p_k) \psi_{\alpha,\lambda}(p_l)}{p_n^2 - P_\alpha^2} V_{lm}(\lambda) . \quad (84)$$

A surprising result is that for unitarily equivalent operators on the grid, such as those generated by the SRG evolution, the phase-shifts computed from the solution of the LS equation are *not* the same; i.e.  $\delta_N^{\text{LS}}(p_n, H) \neq \delta_N^{\text{LS}}(p_n, U_\lambda H U_\lambda^\dagger)$ . This is evident from Eqs. (83) and (84), where we can see explicitly that the LS phase-shifts depend *both* on the eigenvalues  $P_\alpha^2$ , which are isospectral, and the eigenfunctions  $\psi_{\alpha,\lambda}(p_k)$ , which in turn change along the SRG evolution trajectory and so are *not* independent of the SRG cutoff  $\lambda$ . Of course, in the continuum limit one has  $\lim_{N \rightarrow \infty} \delta_N^{\text{LS}}(p_n, H) = \lim_{N \rightarrow \infty} \delta_N^{\text{LS}}(p_n, U_\lambda H U_\lambda^\dagger)$ .

On the other hand, the SRG-evolved potential becomes diagonal in the infrared limit  $\lambda \rightarrow 0$ ,

$$\lim_{\lambda \rightarrow 0} V_{nm}(\lambda) = \delta_{nm} V_n(\lambda \rightarrow 0) , \quad (85)$$

and hence we get

$$V_n(\lambda \rightarrow 0) = R_{nn}(p_n) , \quad (86)$$

such that the infrared fixed-point of the SRG evolution can be related to the energy-shift formula Eq. (80),

$$V_n(\lambda \rightarrow 0) = \frac{(P_n^2 - p_n^2)}{\frac{2}{\pi} w_n p_n^2} = -\frac{\delta^{\text{ES}}(p_n)}{p_n} , \quad (87)$$

thus providing an isospectral definition for the phase-shifts which therefore preserves phase-equivalence along the SRG trajectory. We refer to  $V_n(\lambda \rightarrow 0)$  and  $\delta^{\text{ES}}(p_n)$  as the "eigenpotential" and the "eigenphases" since they are obtained directly from the eigenvalues of the hamiltonian,  $P_n^2$ . It should be mentioned that in the coupled channel case (which actually occurs for the  $^3S_1 - ^3D_1$  Deuteron channel) one needs not only the eigenvalues but also the eigenvectors to determine both the eigenphases and the mixing angles, as discussed in Refs. [33, 34].

### 5.5. Trace Identities and Levinson's theorem

According to Parisi [64] the trace identities are one of the most beautiful results in quantum mechanics. One of the advantages of using the momentum grid basis is the almost straightforward derivation of the finite energy sum rules in potential scattering found in Ref. [37] which are a generalization of the trace identities [64]. While the analyticity of interactions was extensively used there, our derivation is almost completely trivial, and we will just show here some particular examples grasping the basic essence of the approach.

We can compute the following expressions involving the trace of the hamiltonian  $H = T + V$  on a finite momentum grid with  $N$  integration points  $p_n \in [0, \Lambda]$  and weights  $w_n$  ( $n = 1, \dots, N$ ),

$$I_k = \text{Tr} (T + V)^k - \text{Tr} T^k, \quad (88)$$

for any integer  $k$ . On one hand we can saturate with the spectrum including possible bound-states and on the other hand with the momentum states, which yields

$$I_k = \sum_{\alpha} (-\gamma_{\alpha}^2)^k + \sum_n \frac{2}{\pi} w_n p_n^2 p_n^{2k-2} k \left[ -\frac{\delta^{\text{ES}}(p_n)}{p_n} \right] = \sum_{n,m,\dots} \left[ p_n^2 \delta_{nm} + \frac{2}{\pi} w_n p_n^2 V_{nm} \right]^k - \sum_n [p_n^2]^k. \quad (89)$$

For  $k = 1$  we obtain

$$I_1 = \sum_{\alpha} (-\gamma_{\alpha}^2) + \sum_n \frac{2}{\pi} w_n p_n^2 \left[ -\frac{\delta^{\text{ES}}(p_n)}{p_n} \right] = \sum_n \frac{2}{\pi} w_n p_n^2 V_n, \quad (90)$$

which in the continuum yields

$$I_1 \rightarrow \sum_{\alpha} (-\gamma_{\alpha}^2) + \frac{2}{\pi} \int_0^{\Lambda} dp p^2 \left[ -\frac{\delta(p)}{p} \right] = \frac{2}{\pi} \int_0^{\Lambda} dp p^2 V(p, p). \quad (91)$$

In terms of the first Born approximation for the phase-shifts,  $\delta^B(p)$ , this can be written as

$$\sum_{\alpha} (-\gamma_{\alpha}^2) + \frac{2}{\pi} \int_0^{\Lambda} dp p^2 \left[ \frac{-\delta(p) + \delta^B(p)}{p} \right] = 0. \quad (92)$$

This still holds for the finite  $\Lambda$ . Taking the infinite cutoff limit  $\Lambda \rightarrow \infty$  we get the form of the finite energy sum rule of Ref. [37]. Note that our result does not require taking the  $\Lambda \rightarrow \infty$  limit and hence no assumption on analyticity is required for finite  $\Lambda$ .

For  $k = 2$  we obtain

$$I_2 = \sum_{\alpha} (-\gamma_{\alpha}^2)^2 + 2 \sum_n \frac{2}{\pi} w_n p_n^4 \left[ -\frac{\delta^{\text{ES}}(p_n)}{p_n} \right] = 2 \sum_n \frac{2}{\pi} w_n p_n^4 V_n + \sum_{n,m} \left[ \frac{2}{\pi} w_n p_n^2 V_{nm} \right] \left[ \frac{2}{\pi} w_m p_m^2 V_{mn} \right]. \quad (93)$$

Similarly to the case  $k = 1$ , in the continuum this can be written as of Ref. [37] in terms of the second Born approximation for the phase-shifts,  $\delta^{B2}(p)$ ,

$$\sum_{\alpha} (-\gamma_{\alpha}^2)^2 + \frac{4}{\pi} \int_0^{\Lambda} dp p^4 \left[ \frac{-\delta(p) + \delta^{B2}(p)}{p} \right] = 0. \quad (94)$$

The case  $k = 0$  is a bit more tricky and obtained by taking the limit  $k \rightarrow 0$  in Eq. (89),

$$I_0 = \sum_{\alpha} (-\gamma_{\alpha}^2)^0 + \lim_{k \rightarrow 0} \sum_n \frac{2}{\pi} w_n p_n^2 p_n^{2k-2} k \left[ -\frac{\delta^{\text{ES}}(p_n)}{p_n} \right] = \sum_n (1)_{T+V} - \sum_n (1)_T = 0. \quad (95)$$

The last equality just expresses the conservation of dimensions regardless of the interaction. The first term after the first equality is simply the number of bound-states. The term with the phase-shift can be transformed by using the identity  $2k p_n^{2k-2} = dp_n^{2k} / dp_n^2$  going to the continuum and integrating by parts. Thus in the continuum limit

$$N_B + \frac{\delta(\Lambda) - \delta(0)}{\pi} = 0, \quad (96)$$

which becomes the usual Levinson's theorem for  $\Lambda \rightarrow \infty$ . Reinstating the finite momentum grid we get

$$\delta(p_1) - \delta(p_N) = N_B \pi , \quad (97)$$

where  $N_B$  is the number of bound-states allowed by the interaction.

## 6. Numerical results

### 6.1. SRG evolution

We solve the SRG flow equations for the toy model potential numerically on a finite momentum grid with  $N = 50$  gaussian points and a high-momentum UV cutoff  $\Lambda = 2 \text{ fm}^{-1}$ . The discretization of the momentum-space leads to a system of  $N^2$  non-linear first-order coupled differential equations which is solved numerically by using an adaptative variable-step fifth-order Runge-Kutta algorithm. The SRG cutoff  $\lambda$  is varied in a range from 0.05 to  $2.0 \text{ fm}^{-1}$ .

In Fig. 3 we show the SRG evolution of the diagonal and the fully off-diagonal matrix-elements of the toy model potential in the  $^1S_0$  channel using the Wilson and the Wegner generators. As expected, since there are no bound-states in this channel, the SRG evolutions using both generators are nearly identical. As the potential evolves with the SRG cutoff  $\lambda$  the off-diagonal matrix-elements are gradually suppressed such that the potential is driven towards the diagonal form. This can be seen very clearly from the density plots displayed in Fig. 4.

In Fig. 5 we show the SRG evolution of the diagonal and the fully off-diagonal matrix-elements of the toy model potential in the  $^3S_1$  channel using the Wilson and the Wegner generators. For both generators the potential is driven towards a diagonal form though, as expected for the  $^3S_1$  channel, the SRG evolutions become very different when the SRG cutoff  $\lambda$  goes below the critical momentum scale  $\Lambda_c \sim 0.3 \text{ fm}^{-1}$  where the Deuteron bound-state emerges. In the case of the Wilson generator, the low-momentum matrix-elements of the SRG-evolved potential are driven to large negative values, since the Deuteron bound-state is pushed towards the lowest momentum  $p_1$  available on the grid. In the case of the Wegner generator, the Deuteron bound-state decouples from the low-momentum scales when the SRG cutoff  $\lambda$  goes below the critical momentum  $\Lambda_c$  and is placed at a higher momentum  $p_{n_{BS}}$ . We observe in our SRG calculations for the toy model potential on a finite grid that the position at which the bound-state is placed changes when using different values for the number of grid points  $N$  and/or the UV cutoff  $\Lambda$ , similar to what is observed in Ref. [60] for the SRG evolution of LO ChEFT interactions with large momentum cutoffs  $\Lambda_{\text{EFT}}$ , in which the (spurious) bound-state position also changes with the cutoff. Here, for a grid with  $N = 50$  points and  $\Lambda = 2 \text{ fm}^{-1}$ , the bound-state is placed at the momentum  $p_{n_{BS}} = p_9 \sim 0.145 \text{ fm}^{-1}$ . Moreover, the matrix-elements of the SRG-evolved potential corresponding to momenta  $p_n < p_{n_{BS}}$  jump to positive values approaching the  $^3S_1$  channel scattering length  $a_{S_1} = 5.4 \text{ fm}$ . The difference between the SRG evolutions of the toy model potential in the  $^3S_1$  channel using the Wilson and the Wegner generators can be seen very clearly from the density plots displayed in Fig. 6.

### 6.2. SRG regimes

In most studies the convergence pattern of the SRG evolution towards the infrared fixed-point is determined by the stability of single matrix-elements of the evolved potential. This corresponds to a pointwise notion of convergence. However, as we have discussed above, the proper and monotonous decreasing quantities are the operator norms. It is interesting to illustrate to what extent the Frobenius norm and the departure from the infrared limit behave as a function of the SRG cutoff  $\lambda$ . The explicit expression for the Frobenius norm is given by

$$\|V_\lambda\| = \sqrt{\text{Tr } V_\lambda^2(p, p')} , \quad (98)$$

where

$$\begin{aligned} V_\lambda^2(p, p') &= \frac{2}{\pi} \int dq q^2 V_\lambda(p, q) V_\lambda(q, p') , \\ &\simeq \frac{2}{\pi} \sum_{n=1}^N w_n q_n^2 V_\lambda(p, q_n) V_\lambda(q_n, p') . \end{aligned} \quad (99)$$

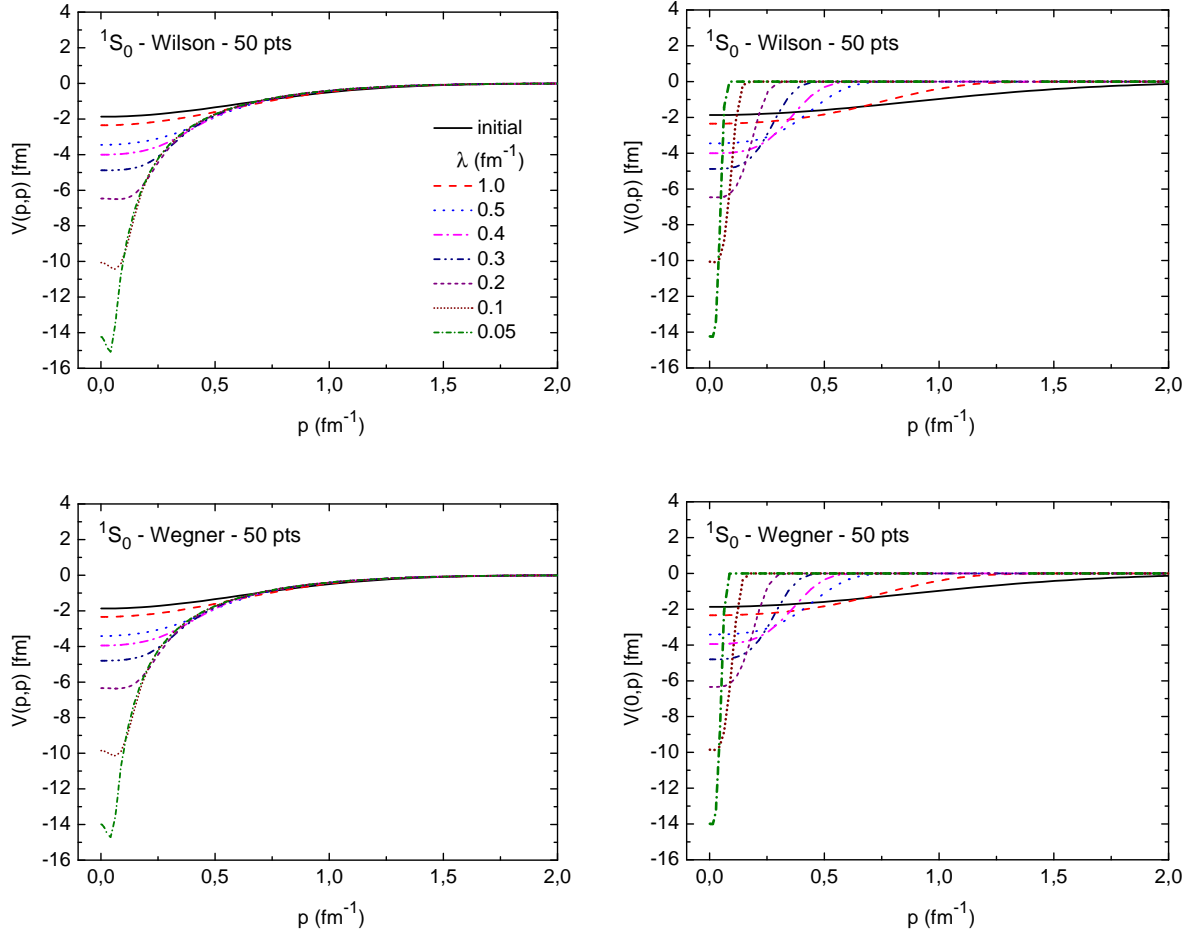


Figure 3: SRG evolution of the toy model separable gaussian potential in the  $^1S_0$  channel ( $N = 50$  and  $\Lambda = 2 \text{ fm}^{-1}$ ) using the Wilson and the Wegner generators. Left panels: diagonal matrix-elements; Right panels: fully off-diagonal matrix-elements.

This is shown in Fig. 7. As one can observe, the stationary condition is reached at about  $\lambda = 0.1 \text{ fm}^{-1}$ . This already provides the relevant scale below which the infrared regime sets in for the finite momentum grid. Actually, the operator norms suggest a new density plot for the quantity

$$\frac{2}{\pi} p p' \sqrt{\Delta p \Delta p'} V_\lambda(p, p') \rightarrow \frac{2}{\pi} p_n p_m \sqrt{w_n w_m} V_\lambda(p_n, p_m), \quad (100)$$

instead of the standard one involving only  $V_\lambda(p, p') \rightarrow V_\lambda(p_n, p_m)$ . These are the normalized SRG-evolved potentials on the grid, according to our previous discussion.

The *weighted* density plots corresponding to Eq. (100) for the SRG evolution of the toy model potential in the  $^1S_0$  and the  $^3S_1$  channels are depicted respectively in Figs. 8 and 9. Note the enhancement of the diagonal region and the suppression of low-energy states as the SRG cutoff  $\lambda$  decreases. This is particularly noticeable around the Deuteron bound-state in the Wegner generator case and around zero momentum in the Wilson generator case. We believe these pictures reflect more faithfully the SRG evolution pattern according to the metric induced by the operator norm relevant for the convergence of the equations.

### 6.3. SRG evolution in the infrared limit and the scattering problem on a finite momentum grid

In the previous sections we have discussed both the SRG flow equations in the infrared limit and the scattering problem on a finite momentum grid independently. In this section we discuss in detail the relation between these

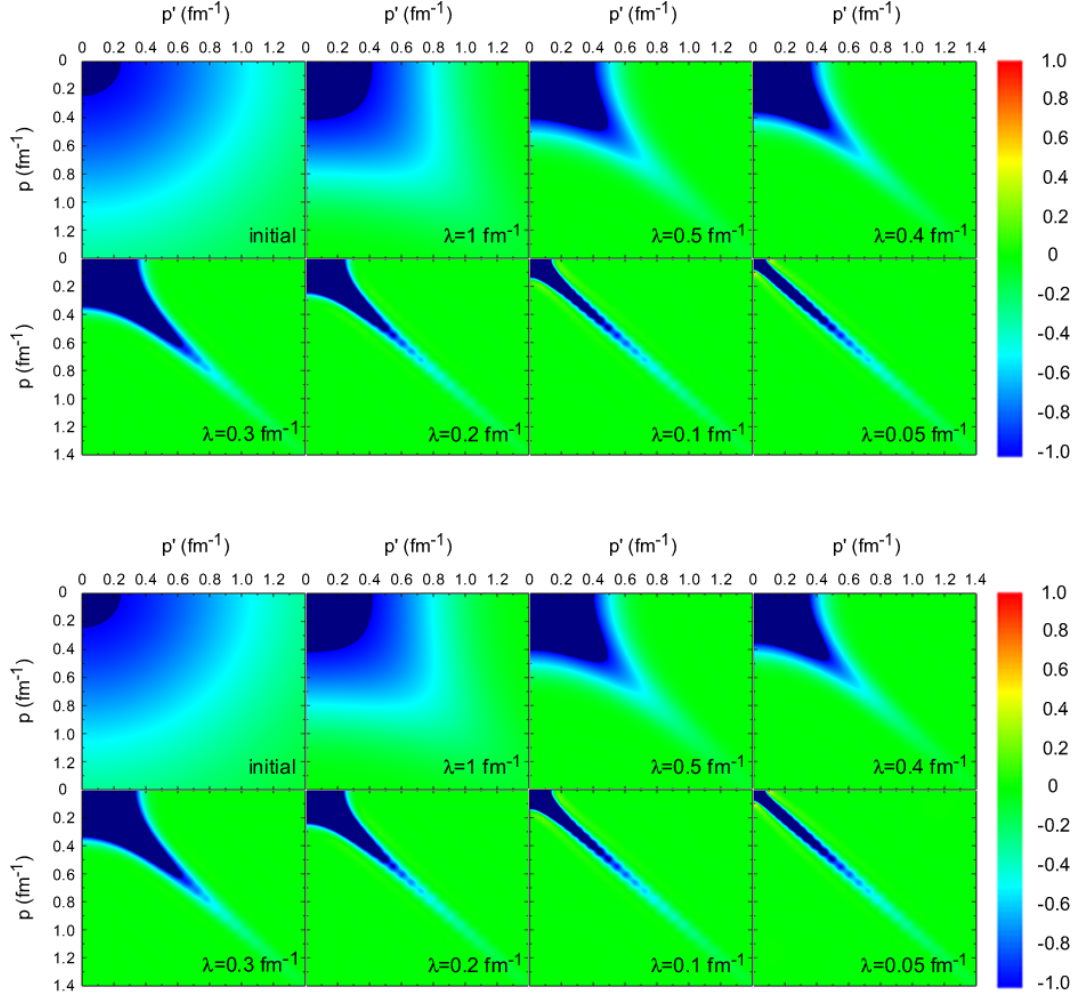


Figure 4: Density plots for the SRG evolution of the toy model separable gaussian potential in the  $^1S_0$  channel ( $N = 50$  and  $\Lambda = 2 \text{ fm}^{-1}$ ) using the Wilson (top panel) and the Wegner (bottom panel) generators.

two apparently disconnected topics through a surprising result involving Levinson's theorem which we have already described in a previous work [23]. As mentioned above the SRG flow equations are isospectral, i.e. they maintain the spectrum of the hamiltonian invariant along the SRG trajectory. Nevertheless, the definition of the spectrum in the continuum requires some care since strictly speaking there is no finite energy-shift but the states become dense. This is illustrated by the finite box quantization formula Eq. (72) together with Eq. (75). Therefore, if we regularize the continuum by a finite momentum grid there appears an inevitable energy-shift due to the interaction and all states in the Hilbert space become normalizable. However, once the finite momentum grid is introduced there is no scattering process and some of the wave operator properties usually assumed for continuum states, such as the intertwining property of the Moller operator, do not hold [65]. Actually, in the case of a hamiltonian allowing for bound-states the energy-shift does not disappear in the continuum. The question is what is the net effect of the energy-shift for positive energy and would-be scattering states when the continuum is approached as a limiting procedure starting from the finite momentum grid.

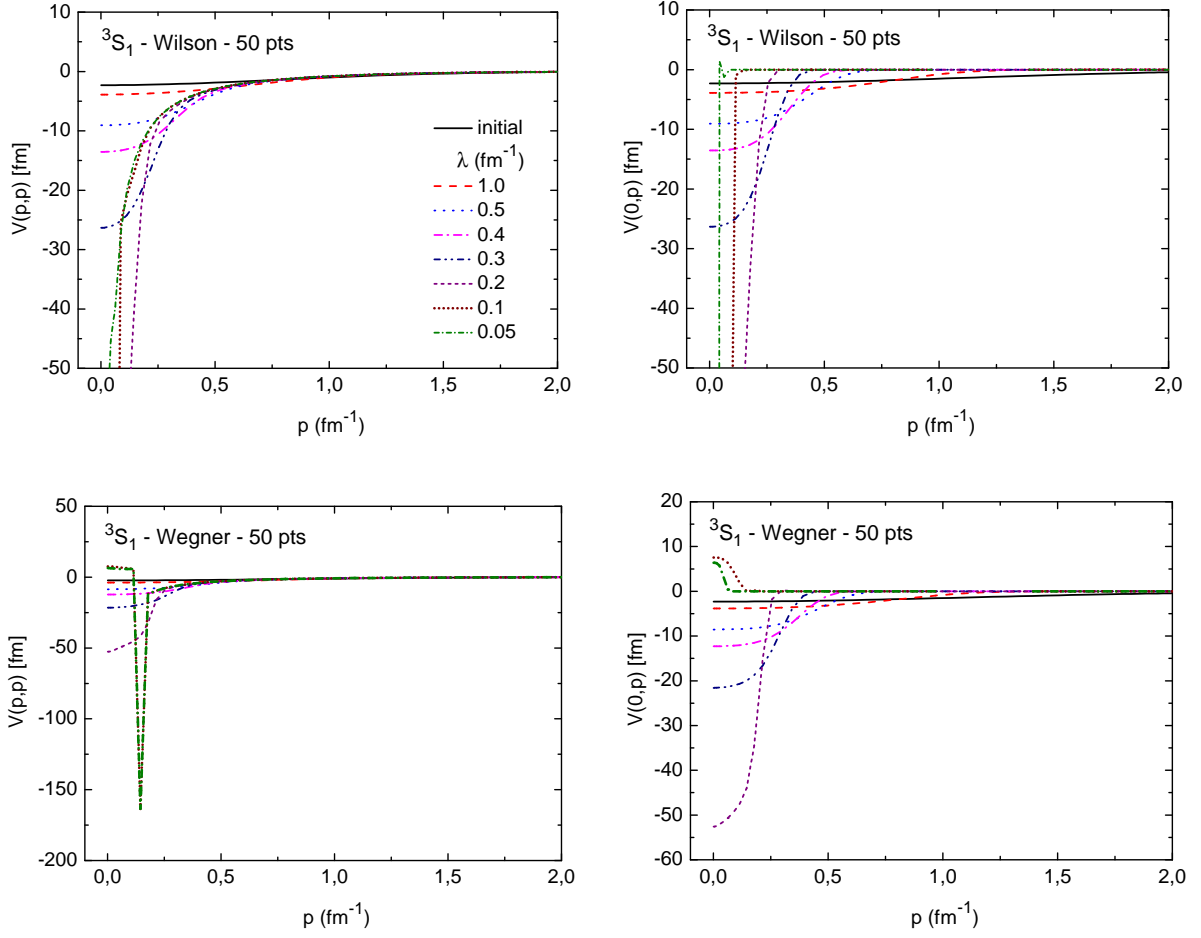


Figure 5: SRG evolution of the toy model separable gaussian potential in the  $^3S_1$  channel ( $N = 50$  and  $\Lambda = 2 \text{ fm}^{-1}$ ) using the Wilson and the Wegner generators. Left panels: diagonal matrix-elements; Right panels: fully off-diagonal matrix-elements.

### 6.3.1. SRG induced ordering of the spectrum and the energy-shift approach

The final ordering of the spectrum induced by the SRG evolution in the infrared limit  $\lambda \rightarrow 0$  can be depicted through the flow of the diagonal matrix-elements of the hamiltonian along the SRG trajectory. In Fig. 10 we show the SRG evolution of the lowest diagonal matrix-elements of the toy model hamiltonian  $H_\lambda(p_n, p_n)$  ( $n = 1, \dots, 6$ ) in the  $^1S_0$  and  $^3S_1$  channels, for a momentum grid with  $N = 20$  points and  $\Lambda = 2 \text{ fm}^{-1}$ . As one can observe, for the  $^1S_0$  channel there is no crossing amongst the diagonal matrix-elements of the hamiltonian evolved with both generators as the SRG cutoff  $\lambda$  approaches the infrared limit, indicating that the initial ascending order is maintained all along the SRG trajectory. For the  $^3S_1$  channel, on the other hand, there are crossings with both generators as the SRG cutoff  $\lambda$  approaches the critical momentum scale  $\Lambda_c \sim 0.3 \text{ fm}^{-1}$ . In the Wilson generator case, the initial ascending order is asymptotically restored in the infrared limit  $\lambda \rightarrow 0$  [25, 38] with the lowest momentum diagonal matrix-element  $H_\lambda(p_1, p_1)$  flowing into the Deuteron bound-state. In the Wegner generator case a re-ordering occurs, such that the diagonal matrix-element  $H_\lambda(p_{n_{BS}}, p_{n_{BS}})$  flows into the Deuteron bound-state in the limit  $\lambda \rightarrow 0$ . For this calculation with  $N = 20$  grid points and  $\Lambda = 2 \text{ fm}^{-1}$  the momentum at which the bound-state is placed on the diagonal of the hamiltonian corresponds to  $p_{n_{BS}} \rightarrow p_5 \sim 0.254 \text{ fm}^{-1}$ . Note that the diagonal matrix-element  $H_\lambda(p_{n_{BS}}, p_{n_{BS}})$  flowing into the Deuteron bound-state is the one that starts to decrease rapidly towards negative values when the SRG cutoff

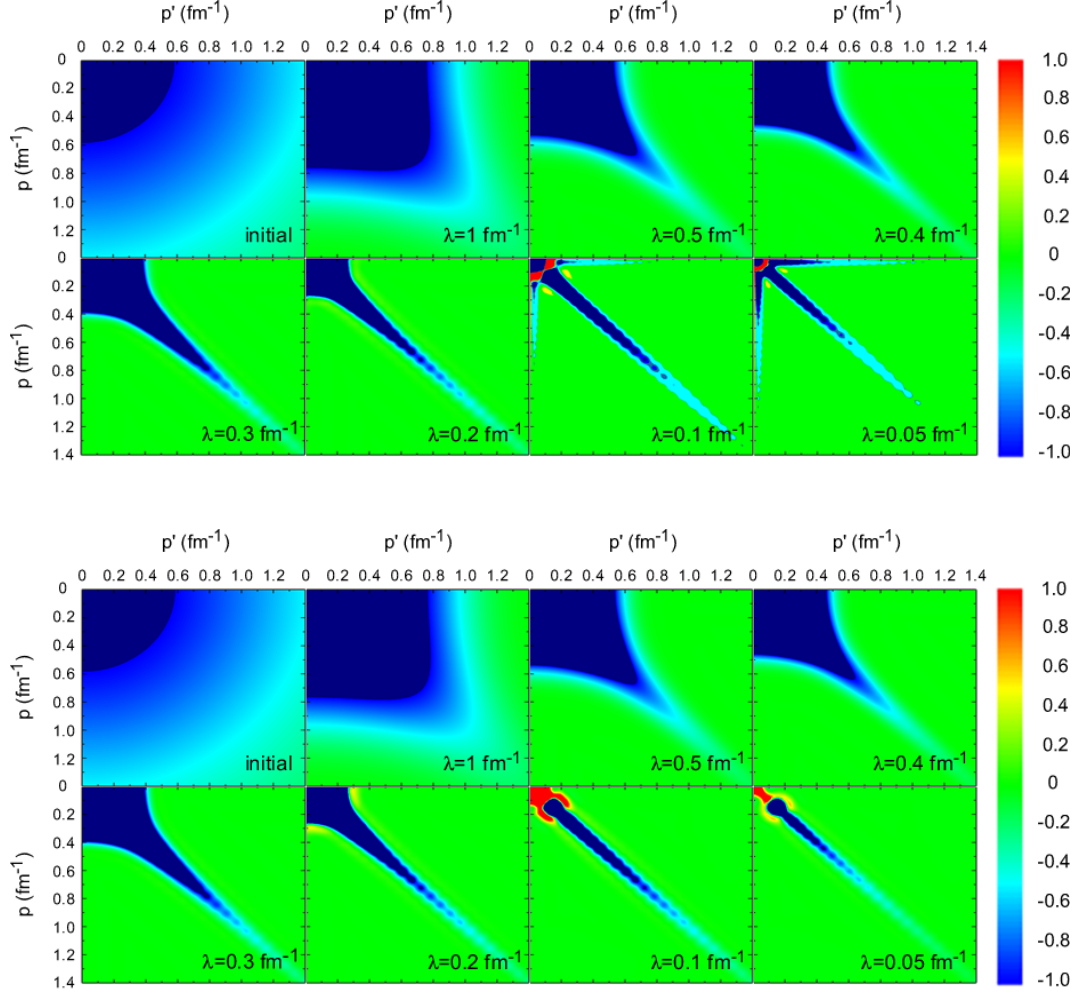


Figure 6: Density plots for the SRG evolution of the toy model separable gaussian potential in the  $^3S_1$  channel ( $N = 50$  and  $\Lambda = 2 \text{ fm}^{-1}$ ) using the Wilson (top panel) and the Wegner (bottom panel) generators.

$\lambda$  approaches  $\Lambda_c$ , indicating the break-up of the kinetic energy dominance, i.e.

$$p_{n_{BS}}^2 < \frac{2}{\pi} w(p_{n_{BS}}) p_{n_{BS}}^2 |V_{\lambda < \Lambda_c}(p_{n_{BS}}, p_{n_{BS}})|. \quad (101)$$

In Fig. 11 we show the diagonal matrix-elements of the toy model potential in the  $^1S_0$  and the  $^3S_1$  channels evolved with both the Wilson and the Wegner generators up to the SRG cutoff  $\lambda = 0.05 \text{ fm}^{-1}$ , compared to the corresponding eigenpotentials  $V_n^{1S_0}(\lambda \rightarrow 0)$  and  $V_n^{3S_1}(\lambda \rightarrow 0)$  evaluated from the energy-shifts through Eq. (87). The eigenpotential  $V_n^{1S_0}(\lambda \rightarrow 0)$  is computed with the eigenvalues arranged in ascending order, which corresponds to the order induced by the SRG evolution in the  $^1S_0$  channel with both generators. The eigenpotential  $V_n^{3S_1}(\lambda \rightarrow 0)$  is computed both with the eigenvalues arranged in ascending order, which corresponds to the order induced by the SRG evolution in the  $^3S_1$  channel with the Wilson generator, and in the order induced by the SRG evolution with the Wegner generator, which is obtained by placing the Deuteron bound-state at  $p_{n_{BS}}$ . As expected by construction, the potentials evolved up to the SRG cutoff  $\lambda = 0.05 \text{ fm}^{-1}$  nearly match the corresponding eigenpotentials. This result clearly shows that the SRG evolved potential indeed converges in the infrared limit  $\lambda \rightarrow 0$  to the eigenpotential  $V_n(\lambda \rightarrow 0)$  computed with the eigenvalues arranged according to the proper SRG induced ordering. Note that for the  $^1S_0$  channel the eigenpotential

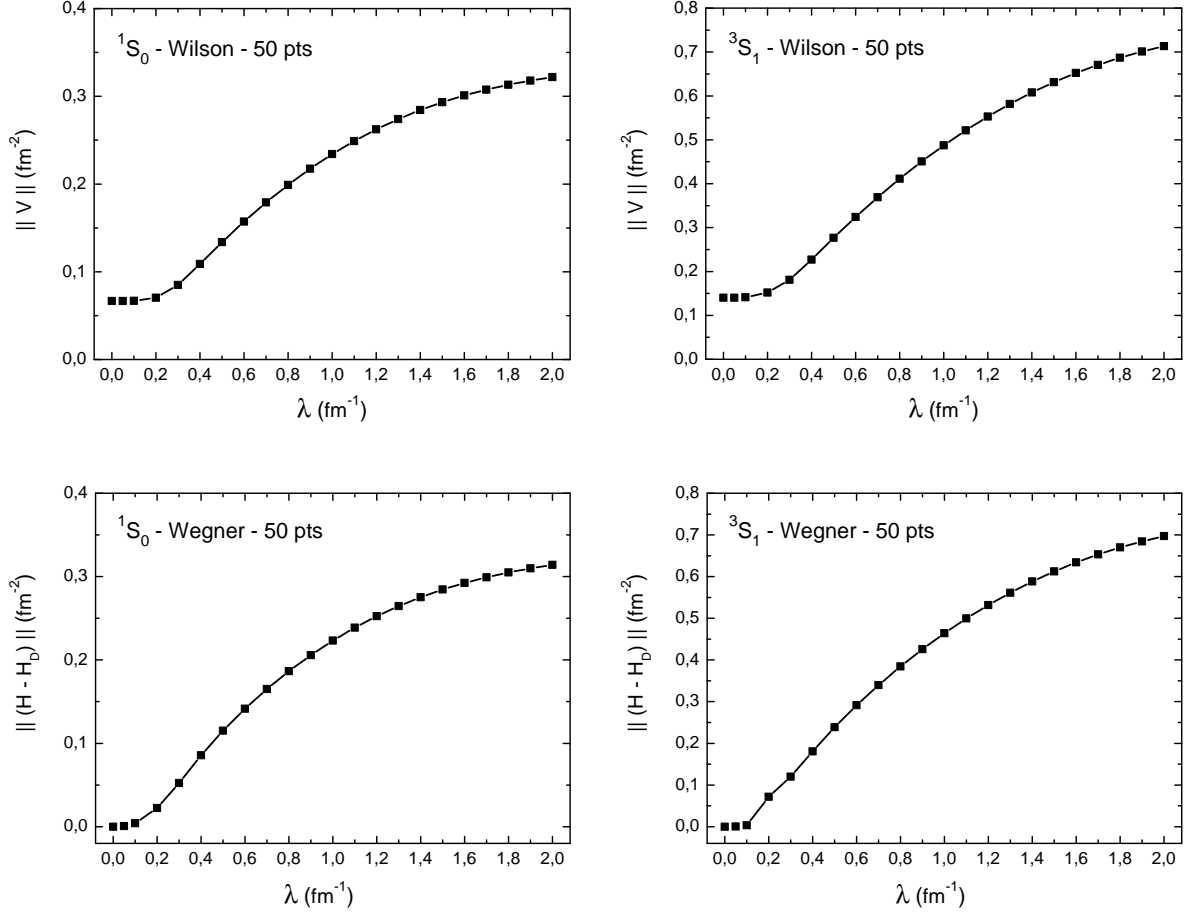


Figure 7: Operator norms for the SRG-evolved toy model separable gaussian potential in the  $^1S_0$  and the  $^3S_1$  channels ( $N = 50$  and  $\Lambda = 2 \text{ fm}^{-1}$ ) for the Wilson and the Wegner generators as a function of the SRG cutoff  $\lambda$ . The infrared regime takes place below  $\lambda \sim 0.1 \text{ fm}^{-1}$ .

at the lowest momentum  $p_1$  on the grid approaches the scattering length, i.e.  $V_1^{1S_0}(\lambda \rightarrow 0) \rightarrow a_{1S_0} = -23.7 \text{ fm}$ , such that the correct behavior at low-momentum in the on-shell limit is obtained. For the  $^3S_1$  channel, on the other hand, the correct behavior, with  $V_1^{3S_1}(\lambda \rightarrow 0) \rightarrow a_{3S_1} = 5.4 \text{ fm}$ , is obtained only when the eigenpotential is computed with the eigenvalues arranged in the order induced by the SRG evolution with the Wegner generator.

### 6.3.2. Ordering prescription and Levinson's theorem

In Fig. 12 we show the phase-shifts  $\delta_\lambda^{\text{LS}}(p_n)$  evaluated from the solution of the LS equation on a finite momentum grid *at the grid points* ( $N = 50$  and  $\Lambda = 2 \text{ fm}^{-1}$ ) for the toy model potential in the  $^1S_0$  and  $^3S_1$  channels evolved through the SRG transformation with the Wilson and the Wegner generators for several values of the SRG cutoff  $\lambda$ . As one can observe, Levinson's theorem [24] is fulfilled on the finite momentum grid for both channels, i.e.

$$\delta_\lambda^{\text{LS}}(p_1) - \delta_\lambda^{\text{LS}}(p_N) = N_B \pi, \quad (102)$$

with  $N_B = 0$  for the  $^1S_0$  channel and  $N_B = 1$  for the  $^3S_1$  channel. However, one can also clearly see that the LS phase-shifts on the finite grid are not independent of the SRG cutoff  $\lambda$ . As pointed out in section 5.4, while the lack of phase-equivalence disappears in the continuum limit, i.e. for  $N \rightarrow \infty$ , the isospectral definition of the phase-shifts on the finite momentum grid based on the energy-shift formula Eq. (80), which we refer to as the *eigenphases*  $\delta^{\text{ES}}(p_n)$ , preserves phase-equivalence along the SRG trajectory for *any* number of grid points  $N$ . Furthermore, as we will show



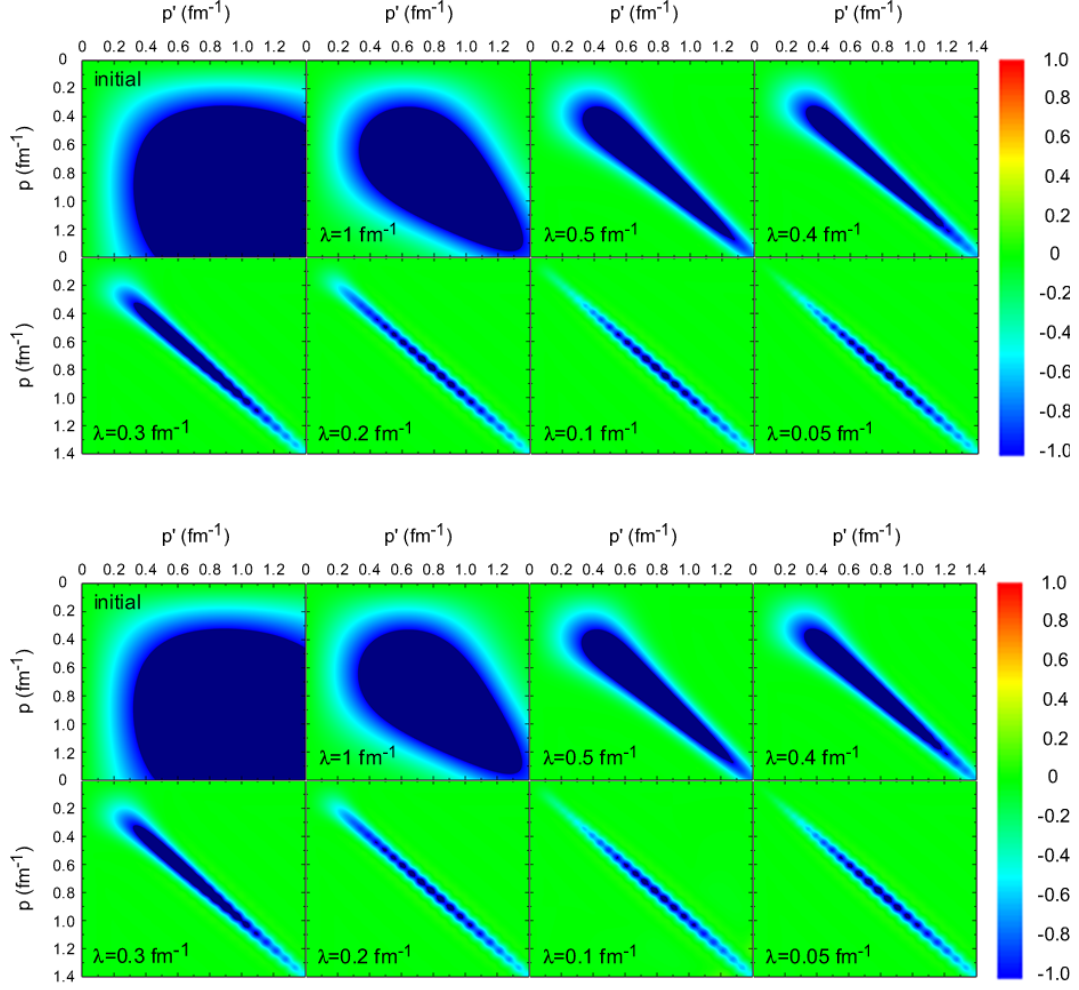


Figure 8: Weighted density plots for the SRG evolution of the toy model separable gaussian potential in the  $^1S_0$  channel ( $N = 50$  and  $\Lambda = 2 \text{ fm}^{-1}$ ) using the Wilson (top panel) and the Wegner (bottom panel) generators.

below, a proper prescription to order the spectrum of  $N$  discrete eigenvalues  $P_n^2$  of the diagonalized hamiltonian when using the energy-shift approach is required to obtain eigenphases which also fulfill Levinson's theorem, particularly when bound-states are allowed by the interaction as in the case of the toy model potential in the  $^3S_1$  channel.

One possible ordering prescription is that derived by Kukulin et al. [33, 34] for a hamiltonian allowing for  $N_B$  bound-states. According to this prescription, the eigenvalues  $P_n^2$  of the hamiltonian are arranged in ascending order and then left-shifted  $N_B$  positions with respect to the eigenvalues  $p_n^2$  of the kinetic energy operator  $T$ , which yields

$$\delta_{\text{Kuk}}^{\text{ES}}(p_n) = -\pi \frac{P_{n+N_B}^2 - p_n^2}{2w_n p_n}, \quad (103)$$

with  $n = 1, \dots, N - N_B$ . Note that Kukulin's prescription implies that the  $N_B$  negative bound-state eigenvalues are just removed, such as to avoid discontinuities in the calculation of the eigenphases.

In the case of the  $^1S_0$  channel there is no need to shift the eigenvalues  $P_n^2$ , since there are no bound-states ( $N_B = 0$ ). Thus, we can evaluate the eigenphases  $\delta^{\text{ES}}(p_n)$  from the energy-shift formula just by arranging the eigenvalues in ascending order, which corresponds to the order induced by the SRG evolution in the  $^1S_0$  channel with both the Wilson and the Wegner generators. The resulting eigenphases for the toy-model potential on a finite momentum grid

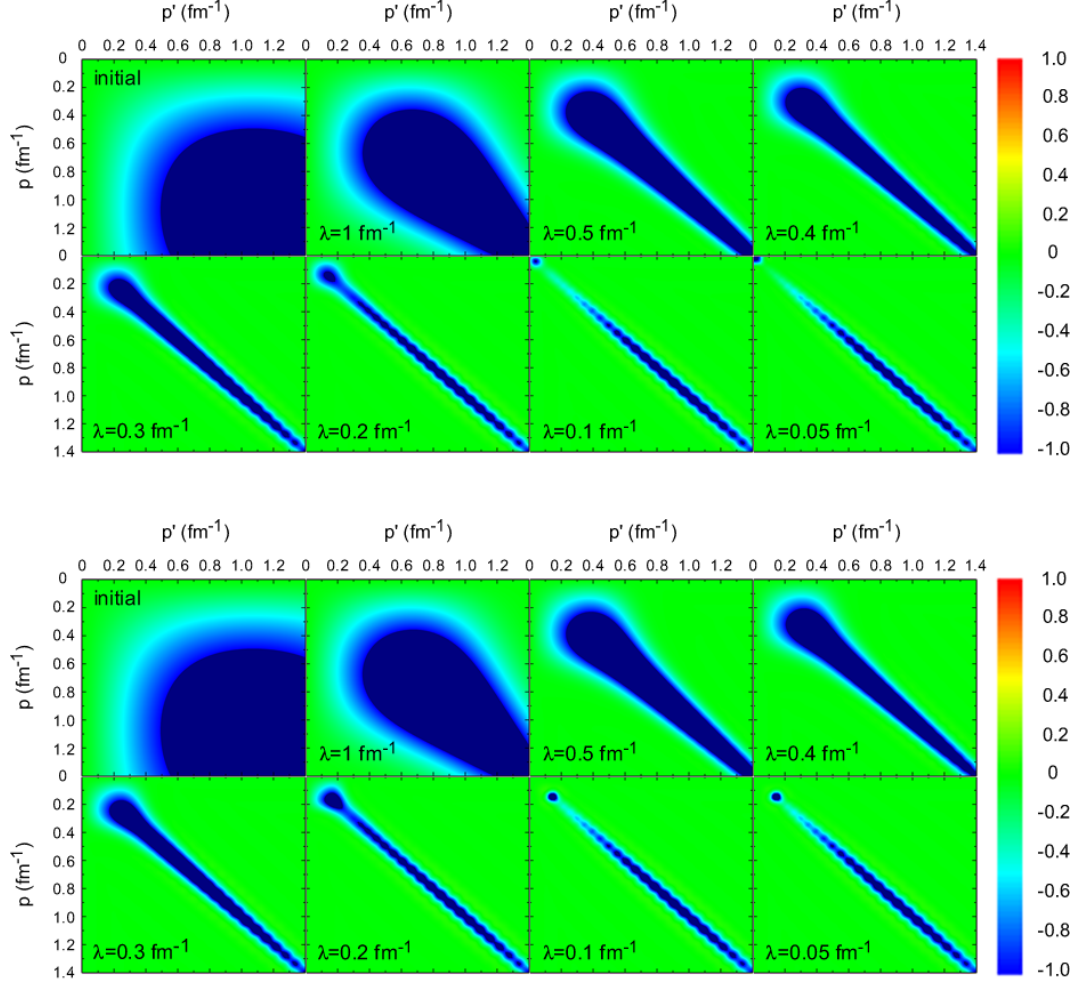


Figure 9: Weighted density plots for the SRG evolution of the toy model separable gaussian potential in the  $^3S_1$  channel ( $N = 50$  and  $\Lambda = 2 \text{ fm}^{-1}$ ) using the Wilson (top panel) and the Wegner (bottom panel) generators.

( $\Lambda = 2 \text{ fm}^{-1}$  and different number of grid points  $N$ ) are shown in Fig. 13, compared to the exact phase-shifts obtained from the solution of the standard LS equation in the continuum limit ( $N \rightarrow \infty$ ). As one can see, the ascending order prescription allows to obtain eigenphases which display the correct behavior in the entire range of momenta, thus complying to Levinson's theorem, i.e.  $\delta^{\text{ES}}(p_1) - \delta^{\text{ES}}(p_N) \sim 0$ .

In the case of the  $^3S_1$  channel, which allows for the Deuteron bound-state ( $N_B = 1$ ), we have considered three different prescriptions to evaluate the eigenphases  $\delta^{\text{ES}}(p_n)$  from the energy-shift formula:

(i) eigenvalues  $P_n^2$  arranged according to Kukulin's prescription, i.e. in ascending order and shifted one position to the left such as to remove the negative Deuteron bound-state eigenvalue.

(ii) eigenvalues  $P_n^2$  arranged according to the order induced by the SRG evolution in the  $^3S_1$  channel with the Wilson generator, i.e. in ascending order, which corresponds to Kukulin's prescription with no left-shifting of the eigenvalues and yields

$$\delta_{\text{Wil}}^{\text{ES}}(p_n) = -\pi \frac{P_n^2 - p_n^2}{2w_n p_n}, \quad (104)$$

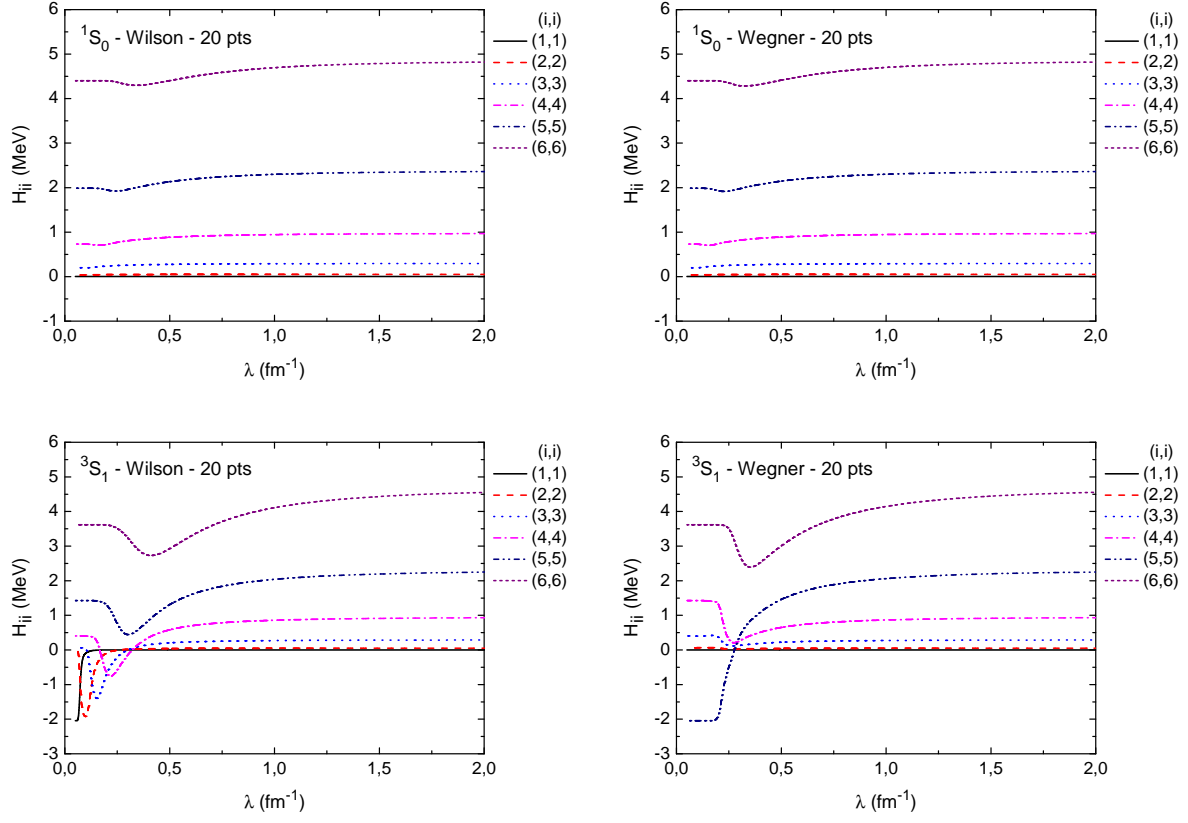


Figure 10: SRG evolution of the lowest diagonal matrix-elements of the toy-model hamiltonian  $H_\lambda(p_n, p_n)$  ( $n = 1, \dots, 6$ ) in the  $^1S_0$  channel and the  $^3S_1$  channel ( $N = 20$  and  $\Lambda = 2 \text{ fm}^{-1}$ ) using the Wilson and the Wegner generators.

Note that in this prescription the negative Deuteron bound-state eigenvalue is placed on the diagonal of the hamiltonian at the lowest momentum on the grid  $p_1$ .

(iii) eigenvalues  $P_n^2$  arranged according to the order induced by the SRG evolution in the  $^3S_1$  channel with the Wegner generator, i.e. with the negative Deuteron bound-state eigenvalue placed at the momentum  $p_{n_{BS}}$  on the diagonal of the hamiltonian and the remaining positive eigenvalues in ascending order. The discontinuity in the eigenphases at the momentum  $p_{n_{BS}}$  can be avoided just by removing the Deuteron bound-state, as in Kukulin's prescription, or by interpolating between the neighboring values, which yields

$$\delta_{\text{Weg}}^{\text{ES}}(p_n) = \begin{cases} -\pi \frac{P_{n+1}^2 - p_n^2}{2w_n p_n} & \text{if } n < n_{BS} \\ -\pi \frac{\bar{P}_{n_{BS}}^2 - p_n^2}{2w_n p_n} & \text{if } n = n_{BS} \\ -\pi \frac{P_n^2 - p_n^2}{2w_n p_n} & \text{if } n > n_{BS} \end{cases} \quad (105)$$

where  $\bar{P}_{n_{BS}}^2 = (P_{n_{BS}+1}^2 + P_{n_{BS}-1}^2)/2$ . Note that in this prescription only the eigenvalues  $P_n^2$  corresponding to momenta  $p_n < p_{n_{BS}}$  are shifted one position to the left.

In Fig. 14 we show the eigenphases for the toy-model potential on a finite momentum grid ( $\Lambda = 2 \text{ fm}^{-1}$  and different number of grid points  $N$ ) evaluated from the energy-shift formula with the eigenvalues  $P_n^2$  of the hamiltonian

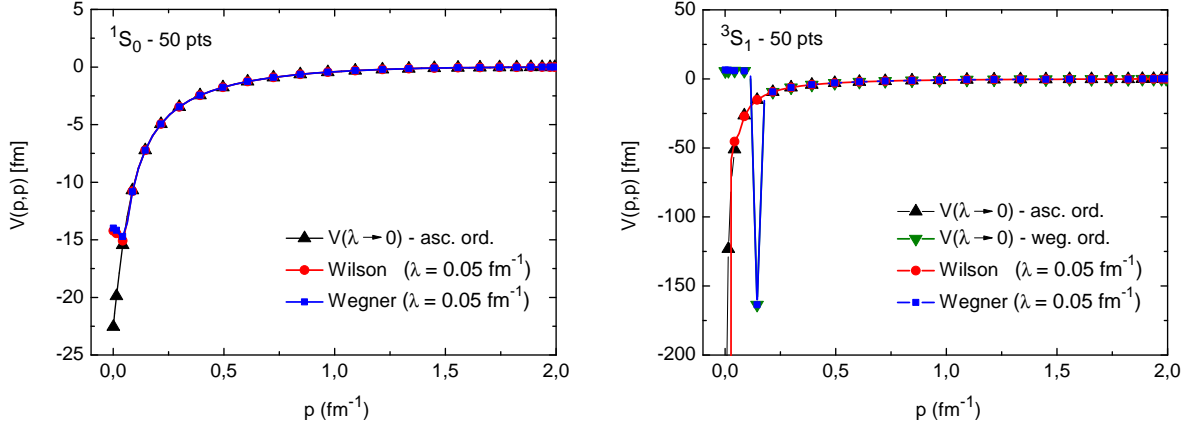


Figure 11: Diagonal matrix-elements of the toy model separable gaussian potential in the  $^1S_0$  channel and the  $^3S_1$  channel ( $N = 50$  and  $\Lambda = 2 \text{ fm}^{-1}$ ) evolved with the Wilson and the Wegner generators up to the SRG cutoff  $\lambda = 0.05 \text{ fm}^{-1}$ . For comparison, we also show the eigenpotentials  $V_n^{1S_0}(\lambda \rightarrow 0)$  and  $V_n^{3S_1}(\lambda \rightarrow 0)$  computed with the eigenvalues arranged according to the corresponding SRG induced orderings.

arranged according to the three prescriptions outlined above, compared to the exact phase-shifts obtained from the solution of the standard LS equation in the continuum limit ( $N \rightarrow \infty$ ). As one can see, the eigenphases obtained with prescription (i) and prescription (ii), which are shown respectively in the top-left and the top-right panels, clearly violate Levinson's theorem. Prescription (i) yields eigenphases which have a proper low-momenta behavior but become distorted at high-momenta due to the left-shifting of the eigenvalues. Prescription (ii), on the other hand, yields eigenphases which have a proper high-momenta behavior but are distorted at low-momenta due to the presence of the Deuteron bound-state<sup>7</sup>. One should note that both in the case of prescription (i) and prescription (ii) the distortion of the eigenphases is generated by a mismatch between the eigenvalues  $P_n^2$  of the hamiltonian and the eigenvalues  $p_n^2$  of the kinetic energy operator  $T$ , respectively at high-momenta and low-momenta. As shown in the bottom-left panel, prescription (iii) yields eigenphases which have a proper behavior both at low-momenta and high-momenta, since the left-shifting is applied *only* to the eigenvalues corresponding to momenta  $p_n < p_{n_{\text{BS}}}$ . As mentioned before, the position  $p_{n_{\text{BS}}}$  of the Deuteron bound-state eigenvalue induced by the SRG evolution with the Wegner generator depends both on the number of grid points  $N$  and the cutoff  $\Lambda$ . In the bottom-right panel, we compare the results obtained with the three prescriptions for  $N = 50$  grid points. As one can see, the eigenphases obtained with prescription (iii) indeed match those obtained with prescription (i) and prescription (ii) respectively for momenta below and above  $p_{n_{\text{BS}}}$ . Thus, we find that the final ordering of the spectrum of discrete eigenvalues  $P_n^2$  of the toy-model hamiltonian induced by the SRG evolution with the Wegner generator in the infrared limit ( $\lambda \rightarrow 0$ ) remarkably provides a prescription which allows to obtain isospectral phase-shifts from the energy-shift formula that comply to Levinson's theorem in the presence of the Deuteron bound-state.

The effectiveness of ordering prescription (iii) can be traced to the decoupling of the Deuteron bound-state from the low-momentum scales when the toy-model potential in the  $^3S_1$  channel is evolved through the SRG transformation using the Wegner generator. The key point is that by placing the Deuteron bound-state eigenvalue at the position  $p_{n_{\text{BS}}}$  induced by the SRG evolution with the Wegner generator in the infrared limit ( $\lambda \rightarrow 0$ ) we obtain eigenphases from the energy-shift formula which display the correct behavior in the entire range of momenta (within the expected uncertainties of the finite momentum grid). One should note, however, that such an ordering does not necessarily correspond to the optimal one. We have evaluated the eigenphases  $\delta^{\text{ES}}(p_n)$  for the toy model potential in the  $^3S_1$  channel on a finite momentum grid ( $\Lambda = 2 \text{ fm}^{-1}$  and different number of grid points  $N$ ) using prescription (iii) but varying the position of the Deuteron bound-state eigenvalue  $p_{n_{\text{BS}}}$ , and compared the results to the exact phase-shifts obtained from the solution of the standard LS equation in the continuum limit ( $N \rightarrow \infty$ ). By computing the

<sup>7</sup>The point corresponding to the lowest momentum  $p_1$  on the grid, at which the Deuteron bound-state eigenvalue is placed on the diagonal of the hamiltonian, is out of scale and so is omitted from the plot.

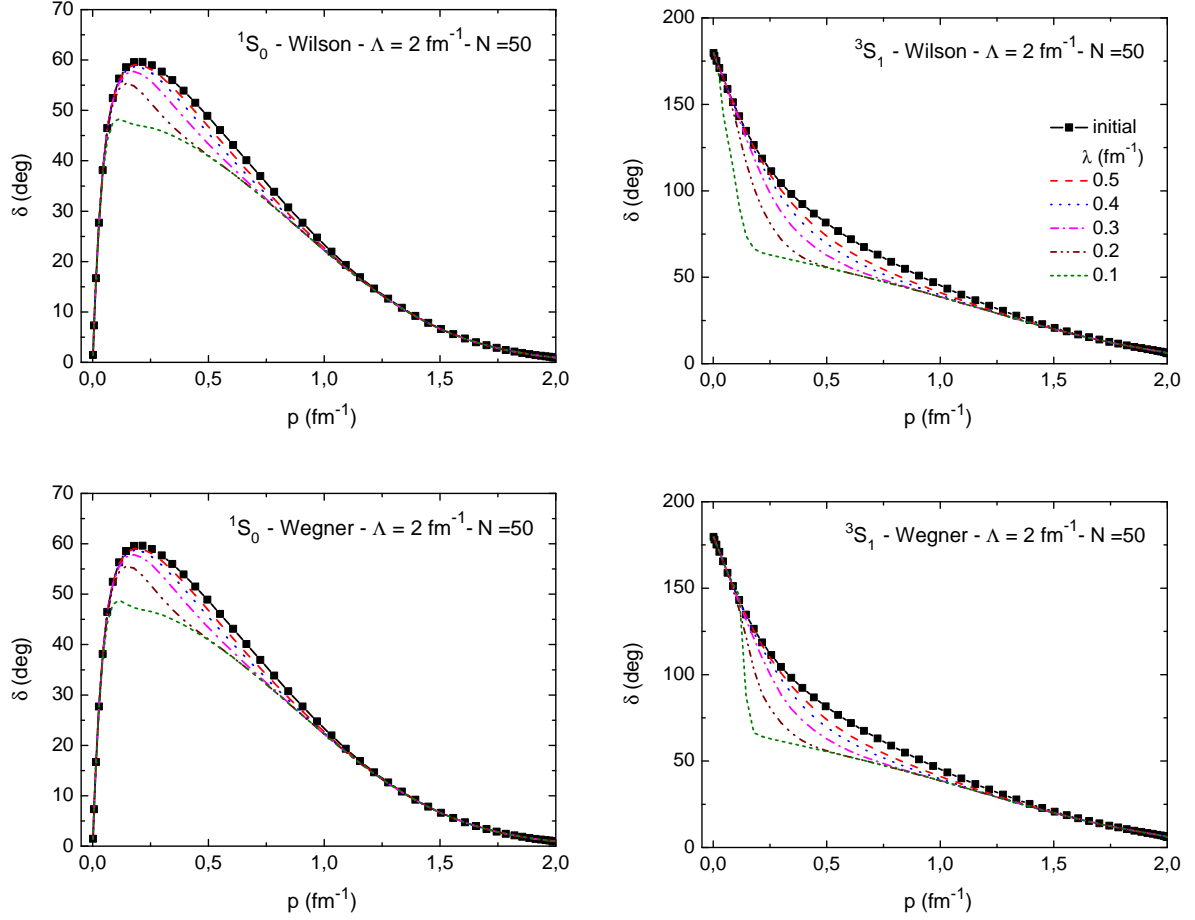


Figure 12: Phase-shifts  $\delta_L^S(p_n)$  evaluated from the solution of the LS equation on a finite momentum grid *at the grid points* ( $\Lambda = 2 \text{ fm}^{-1}$  and  $N = 50$ ) for the toy model separable gaussian potential in the  $^1S_0$  and  $^3S_1$  channels evolved through the SRG transformation with the Wilson and the Wegner generators for several values of the SRG cutoff  $\lambda$ .

corresponding root mean square (RMS) errors as a function of  $p_{n_{BS}}$ , we find that for each value of the number of grid points  $N$  there is a well-defined minimum. As one can see in Fig. 15, the position  $p_{n_{BS}}^{\text{opt}}$  minimizing the RMS errors, which seems to converge in the continuum limit to the characteristic Deuteron momentum scale  $\gamma = 0.23 \text{ fm}^{-1}$ , is different from that induced by the SRG evolution with Wegner generator in the infrared limit.

As pointed out before, the final ordering of the spectrum induced by the SRG evolution in the infrared limit may depend on the choice of the SRG generator when bound-states are allowed by the interaction. In this way, it is possible that a specific generator exists for which the position of the Deuteron bound-state induced by the SRG evolution corresponds to  $p_{n_{BS}}^{\text{opt}}$ , thus providing the optimal ordering prescription for the energy-shift approach.

## 7. Consequences of the fixed points for nuclear binding: Triton and Helium nuclei

The ambiguities arising from off-shell uncertainties has been the main source of problems in Nuclear Physics calculations. There are a variety of  $NN$  potentials in the literature providing a high-quality description of scattering data and Deuteron properties. They produce, however, different results when comparing to nuclear matter and nuclear structure calculations. So far, we have dealt with the two-body problem. Of course, much of the motivation to undertake the SRG evolution concerns the applications to nuclear structure. Our purpose here is to illustrate the different implications of the SRG using the Wegner and the Wilson generators along the lines discussed above using

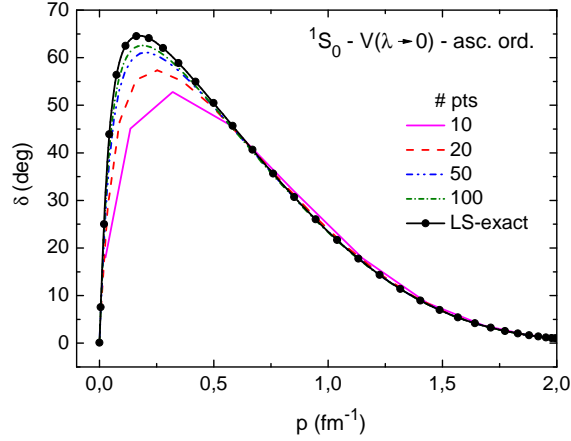


Figure 13: Eigenphases  $\delta^{\text{ES}}(p_n)$  for the toy-model separable gaussian potential in the  $^1S_0$  channel on a finite momentum grid ( $\Lambda = 2 \text{ fm}^{-1}$  and different number of grid points  $N$ ) evaluated from the energy-shift formula with the eigenvalues arranged in ascending order. For comparison, we also show the exact phase-shifts obtained from the solution of the standard LS equation in the continuum limit ( $N \rightarrow \infty$ ).

our simple toy model potential. Most calculations in Nuclear Physics use a mean field reference state, which is often a harmonic oscillator (HO) shell-model state, upon which correlations are built, namely  $|\Psi\rangle = U|\phi\rangle$ , where  $U$  is some unitary transformation. The SRG interpretation is that correlations are shifted from the reference state to the interaction via the unitary transformation  $U$ .

Within the shell-model we will restrict to the cases with  $A = 3$  and  $A = 4$ , which correspond respectively to the Triton and the  $\alpha$ -particle, as only  $S$ -wave interactions are required. In order to simplify matters as much as possible we will describe the states as  $t \equiv (1s)^3$  and  $\alpha \equiv (1s)^4$  respectively,

$$\psi_{t,\uparrow}(p_1, p_2, p_3) \equiv \left[ \prod_{i=1}^3 \varphi_{1s}(p_i) \right] \mathcal{A}(p \uparrow, n \uparrow, n \downarrow), \quad (106)$$

$$\psi_{t,\downarrow}(p_1, p_2, p_3) \equiv \left[ \prod_{i=1}^3 \varphi_{1s}(p_i) \right] \mathcal{A}(p \downarrow, n \uparrow, n \downarrow), \quad (107)$$

$$\psi_{\alpha}(p_1, p_2, p_3, p_4) \equiv \left[ \prod_{i=1}^4 \varphi_{1s}(p_i) \right] \mathcal{A}(p \uparrow, n \uparrow, p \downarrow, n \downarrow), \quad (108)$$

where  $\mathcal{A}$  is a normalized antisymmetrizer and  $\varphi_{1s}$  is the HO –  $1s$  wave-function with a  $b$  parameter, given by

$$\sqrt{\frac{2}{\pi}} \varphi_{1s}(p) = \frac{2 \sqrt{b^3} e^{-\frac{1}{2} b^2 p^2}}{\sqrt{\pi}}. \quad (109)$$

The energy calculation for the  $A = 3$  and  $A = 4$  systems at rest,  $\sum_{i=1}^A p_i = 0$ , is straightforward and reads

$$\{E_t(\lambda), E_{\alpha}(\lambda)\} = \{-B_t, -B_{\alpha}\} = \min_b \left[ (A-1) \left\langle \frac{p^2}{2M} \right\rangle_{1s} + \frac{A(A-1)}{2} \frac{1}{2} \langle V_{1S_0,\lambda} + V_{3S_1,\lambda} \rangle_{\text{rel},1s} \right] \Big|_{A=3,4}. \quad (110)$$

The single particle kinetic energy reads

$$\left\langle \frac{p^2}{2M} \right\rangle_{1s} = \frac{2}{\pi} \int_0^{\infty} p^2 dp [\varphi_{1s}(p)]^2 \frac{p^2}{2M}, \quad (111)$$

and the potential matrix-element is defined as

$$\langle \phi_{\text{rel}} | V_{\lambda} | \phi_{\text{rel}} \rangle = \frac{2}{\pi} \int_0^{\infty} dp [p^2 \phi_{\text{rel}}(p)] \frac{2}{\pi} \int_0^{\infty} dp' [p'^2 \phi_{\text{rel}}(p')] V_{\lambda}(p', p), \quad (112)$$

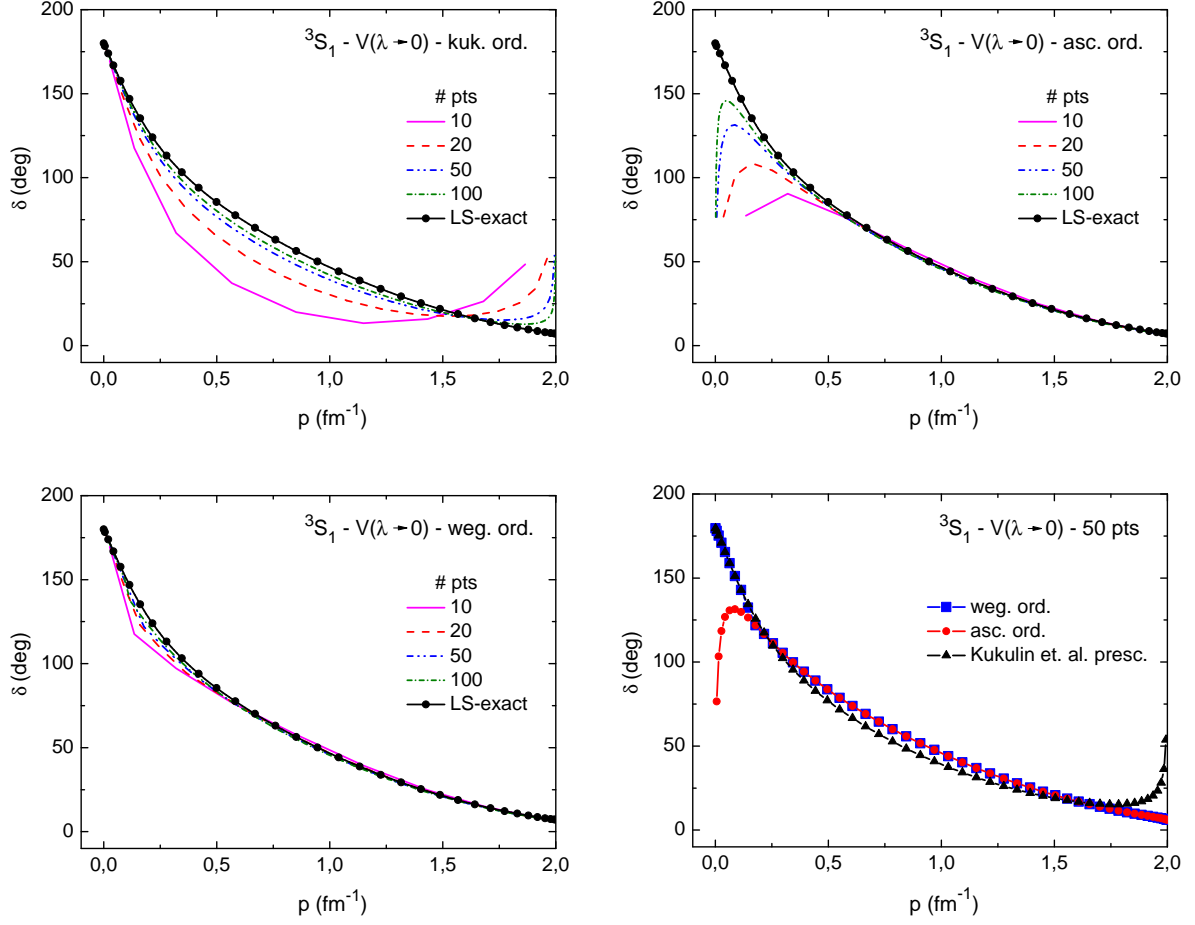


Figure 14: Eigenphases  $\delta^{\text{ES}}(p_n)$  for the toy model separable gaussian potential in the  $^3S_1$  channel on a finite momentum grid ( $\Lambda = 2 \text{ fm}^{-1}$  and different number of grid points  $N$ ) evaluated from the energy-shift formula with the eigenvalues arranged according to Kukulin's prescription (i), the order induced by the SRG evolution with the Wilson generator (ii), i.e. in ascending order, and the order induced by the SRG evolution with the Wegner generator (iii). For comparison, we also show the exact phase-shifts obtained from the solution of the standard LS equation in the continuum limit ( $N \rightarrow \infty$ ). In the bottom-right panel we compare the results obtained with prescriptions (i), (ii) and (iii) for  $N = 50$  grid points.

where the *relative* wave function is given by (note the  $\sqrt{2}$  factor),

$$\phi_{\text{rel}}(p) = \varphi_{1s}(p, b/\sqrt{2}) . \quad (113)$$

Eq. (110) can be interpreted in terms of the number of pairs in the  $^1S_0$  and  $^3S_1$  states being  $n_{1S_0, t} = n_{3S_1, t} = 3/2$  for the Triton and  $n_{1S_0, \alpha} = n_{3S_1, \alpha} = 6/2$  for the  $\alpha$ -particle.

Within this shell-model calculation scheme we may also define a variational Deuteron energy,

$$E_d(\lambda) = \min_b \langle p^2/M + V_{3S_1, \lambda} \rangle_{\text{rel}, 1s} , \quad (114)$$

which unlike the exact one will depend on the SRG cutoff  $\lambda$ . For  $\lambda \rightarrow \infty$  the Deuteron is unbound by 0.2 MeV, and the binding-energy obtained for the Triton is  $B_t^{\text{Var}} = 5.9661 \text{ MeV}$  to be compared with the exact Faddeev equation result  $B_t = 6.65543 \text{ MeV}$ , whereas the  $\alpha$ -particle yields  $B_\alpha^{\text{Var}} = 32.1054 \text{ MeV}$ .

It is interesting to analyze the SRG evolution from  $\lambda \rightarrow \infty$  down to  $\lambda \rightarrow 0$ , disregarding here explicit three-body or four-body forces (see Ref. [25] for some further details on this issue). In Fig. 16 we see the effect of the SRG evolution on a simple variational calculation for the cases with  $A = 2, 3, 4$ . Here and for illustration purposes we take

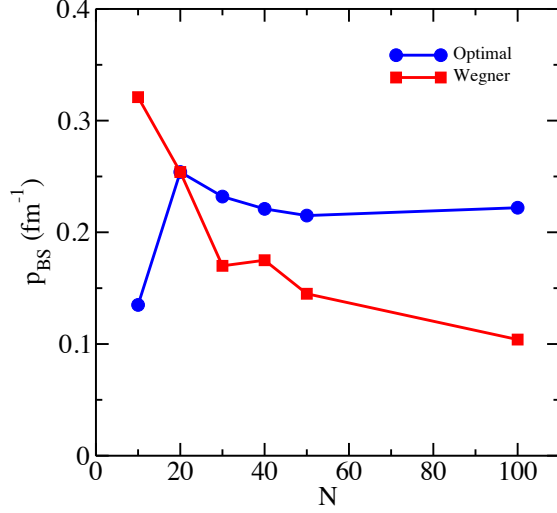


Figure 15: Comparison between the position of the Deuteron bound-state which minimizes the RMS errors in the eigenphases  $\delta^{\text{ES}}(p_n)$  with respect to the exact phase-shifts obtained from the solution of the standard LS equation in the continuum limit ( $N \rightarrow \infty$ ) and the position induced by the SRG evolution with the Wegner generator in the infrared limit ( $\lambda \rightarrow 0$ ), for different number of grid points  $N$ .

a grid with  $\Lambda = 2 \text{ fm}^{-1}$  and  $N = 50$  gauss points. A very similar behavior in the region  $\lambda \gtrsim 1 \text{ fm}^{-1}$  is found for both the Wilson and the Wegner generators. However, as we can see, in the region of small  $\lambda$  the behavior for the Wilson and the Wegner generators is quite different and, near  $\lambda \sim 0.2 \text{ fm}^{-1}$ , a clear jump in the energies is observed. To understand how this surprising result comes about let us consider the calculation of the energy in further detail for the finite momentum grid which is used for the SRG evolution. The kinetic and potential energy contributions become

$$\left\langle \frac{p^2}{2M} \right\rangle_{1s} \rightarrow \frac{2}{\pi} \sum_n w_n p_n^2 \frac{p_n^2}{M} \phi_{N,\text{rel}}(p_n)^2 \quad (115)$$

and

$$\langle \phi_{\text{rel}} | V_\lambda | \phi_{\text{rel}} \rangle \rightarrow \left( \frac{2}{\pi} \right)^2 \sum_{n,m} w_n w_m [p_n^2 \phi_{\text{rel},N}(p_n)] [p_m^2 \phi_{\text{rel},N}(p_m)] V_{nm}(\lambda) . \quad (116)$$

The HO – 1s states need to be renormalized on the grid as follows,

$$\varphi_{1s,N}(p_n) = Z_N \varphi_{1s}(p_n) , \quad Z_N^2 = \frac{2}{\pi} \sum_n w_n p_n^2 [\varphi_{1s}(p_n)]^2 . \quad (117)$$

If one takes the infrared limit  $\lambda \rightarrow 0$ , the potential becomes diagonal and one gets

$$\langle \phi_{\text{rel}} | V_{\lambda \rightarrow 0} | \phi_{\text{rel}} \rangle \rightarrow \left( \frac{2}{\pi} \right)^2 \sum_n w_n^2 p_n^4 \phi_{\text{rel}}(p_n)^2 V_n(\lambda \rightarrow 0) . \quad (118)$$

We see the weight squared factor  $w_n^2$  and *naively* in the  $\Lambda$ -fixed and  $N \rightarrow \infty$  continuum limit, we obtain

$$V(N \rightarrow \infty) = \langle \phi_{\text{rel}} | V_{\lambda \rightarrow 0} | \phi_{\text{rel}} \rangle_{N \rightarrow \infty} \rightarrow \left( \frac{2}{\pi} \right) \frac{\Lambda}{N} \int_0^\Lambda p^4 \phi_{\text{rel}}(p)^2 \left[ \frac{-\delta(p)}{p} \right] \rightarrow 0 , \quad (119)$$

regardless on the HO parameter  $b$ . Thus, the kinetic energy gets minimal for  $b \rightarrow \infty$  and hence the minimum takes place at zero energy. While this argument agrees with the behavior for the Wegner generator observed in Fig. 16 it



fails to reproduce the trend found for the Wilson generator. The flaw in the argument can be seen more clearly in the Deuteron case, where

$$\lim_{\lambda \rightarrow 0} E_d(\lambda) = \frac{2}{\pi} \sum_n w_n p_n^2 \frac{P_n^2}{M} \phi_{\text{rel},N}(p_n)^2 . \quad (120)$$

Note that with the exception of the Deuteron state  $P_d^2 = -\gamma_d^2$  all others fulfill  $P_n^2 > 0$ . The difference, however, is in the location of the bound-state after the SRG evolution. The bound-state is located at the lowest point on the grid for the Wilson generator and at some intermediate point for the Wegner generator,

$$P_d^2 = P_1^2 \quad (\text{Wilson generator}) \quad \text{and} \quad P_d^2 = P_{n_B}^2 \quad (\text{Wegner generator}) . \quad (121)$$

However, the trial wave function is peaked at the origin, which on the finite momentum grid corresponds to the lowest momentum  $p_1$ . Using the fact that all  $P_n^2 > 0$  with the exception of the bound-state we obtain

$$\lim_{\lambda \rightarrow 0} E_d(\lambda) \geq \frac{2}{\pi} w_1 p_1^2 \frac{P_1^2}{M} \phi_{\text{rel},N}(p_1)^2 = -\frac{\gamma_d^2}{M} \frac{w_1 p_1^2 e^{-p_1^2 b^2}}{\sum_n w_n p_n^2 e^{-p_n^2 b^2}} \rightarrow -\frac{\gamma_d^2}{M} \quad (\text{Wilson generator}) , \quad (122)$$

$$\lim_{\lambda \rightarrow 0} E_d(\lambda) \geq \frac{2}{\pi} w_{n_B} p_{n_B}^2 \frac{P_{n_B}^2}{M} \phi_{\text{rel},N}(p_{n_B})^2 = -\frac{\gamma_d^2}{M} \frac{w_{n_B} p_{n_B}^2 e^{-p_{n_B}^2 b^2}}{\sum_n w_n p_n^2 e^{-p_n^2 b^2}} \rightarrow 0 \quad (\text{Wegner generator}) . \quad (123)$$

Of course, this argument holds in the infrared limit  $\lambda \rightarrow 0$ . A qualifying remark here becomes necessary: a distinction between the infrared limit  $\lambda \rightarrow 0^+$  and the value  $\lambda = 0$  should be made as we are dealing with variational wave functions. For finite  $\lambda$ , as long as the bound-state is not either shifted or anchored at some fixed place, the behavior for both generators will not essentially differ. The dramatic evolution of the potential can be more clearly seen by inspecting the sequence previously displayed. We see that the jump in the Deuteron energy in the case of the Wegner generator is directly related to the crossing of the hamiltonian diagonal matrix-element corresponding to the bound-state. A similar argument for the variational shell-model calculations for the cases with  $A = 3$  and  $A = 4$  yields the results

$$\lim_{\lambda \rightarrow 0} E_d(\lambda) = -B_d , \quad \lim_{\lambda \rightarrow 0} E_t(\lambda) = -\frac{3}{2} B_d , \quad \lim_{\lambda \rightarrow 0} E_\alpha(\lambda) = -3B_d , \quad (\text{Wilson generator}) , \quad (124)$$

$$\lim_{\lambda \rightarrow 0} E_d(\lambda) = 0 , \quad \lim_{\lambda \rightarrow 0} E_t(\lambda) = 0 , \quad \lim_{\lambda \rightarrow 0} E_\alpha(\lambda) = 0 , \quad (\text{Wegner generator}) , \quad (125)$$

which is checked by the numerical calculations as shown in Fig. 16. Note that the only contribution in the infrared limit  $\lambda \rightarrow 0$  stems in this case from the two-body bound-state. The continuum contributions in both the  $^1S_0$  and  $^3S_1$  channels vanish.

For completeness, let us mention that as we evolve along the SRG trajectory we also find linear correlations in two regimes

$$\Delta B_\alpha / \Delta B_t \sim 2 \quad (\lambda \rightarrow 0) \quad \text{and} \quad \Delta B_\alpha / \Delta B_t \sim 4 \quad (\lambda \sim 1) . \quad (126)$$

The corresponding Tjon-lines are depicted in Fig. 17. The gap in the Wegner generator case can be clearly identified. We compare with the asymptotic lines  $E_\alpha = 4E_t - 3E_d$  and  $E_\alpha = 2E_t$  which were identified in our previous work [25] invoking three-body forces. The extrapolation of this formula gives  $B_\alpha = 4 \times 8.482 - 3 \times 2.225 = 27.53$  MeV, while the experimental value is  $B_\alpha^{\text{exp}} = 28.296$  MeV. As we see, the sharp intersection between the two lines happens exactly at the SRG cutoff  $\lambda$  where the jumps in the binding energies are observed in Fig. 16, which corresponds to the critical values  $E_t = 3E_d/2$  and  $E_\alpha = 3E_d$ . The phenomenon we observe resembles closely an avoided crossing pattern, a phenomenon familiar from molecular physics in the Born-Oppenheimer approximation [66], where the adiabatic parameter is the Triton binding-energy,  $E_t$ . As we see, the variational calculation takes the minimal energy from the two possible branches in the Wilson generator case since the variational  $(1s)^4$  state for the  $\alpha$ -particle contains  $dd$  states with opposite spin polarization at rest. Hence, the critical point corresponds to the break up process  $\alpha \rightarrow dd$ . As we see from Fig. 17, this break-up component is absent in the Wegner generator case and one jumps to the free  $4N$  state at rest at  $\lambda \rightarrow 0$ .

Our results generate a Tjon-line, with a slope 4 for the SRG cutoff below  $\lambda \sim 1\text{fm}^{-1}$ . We remind that this is the regime which so far remained inaccessible for realistic interactions, basically due to numerical difficulties triggered by the long momentum tail of the potentials. Of course, while the generic features found here are expected to become universal as we approach the infrared, the accuracy of our results regarding the specific implications for nuclear binding should be tested, particularly since our solution is just a variational approximation. A thorough analysis of both the  $A = 3, 4, 16, 40$  as well as neutron and nuclear matter extending preliminary results for realistic potentials [21] along the present lines will be presented elsewhere.

## 8. Summary, conclusions and outlook

The SRG flow equations provide an example of an isospectral flow, i.e. a transformation which preserves the eigenvalues of the hamiltonian but rotates the eigenfunctions in such a way that transition matrix elements are increasingly and exponentially suppressed in the corresponding energy differences. This approach has offered new opportunities in Nuclear Physics as it allows the possibility of describing phase-equivalent interactions which conveniently become more diagonal. The practical implementation of the SRG approach usually requires a discretization in momentum space.

Our analysis has therefore been performed on a finite momentum grid which makes the problem computationally manageable but also leads to specific features related to the formulation of the scattering problem. In particular two unitarily equivalent hamiltonians do not provide the same phase-shifts obtained by the solution of the LS equation on the grid. Therefore, we have adopted the energy-shift definition of the discretized Hamiltonian suggested many years ago by Lifschits and extensively developed by Kukulín *et al.* in more recent years within the context of the few-body problem. We have found suitable formulas correctly incorporating Levinson's theorem. As a by-product we have also deduced momentum grid based generalized trace identities or finite energy sum rules put forward by Jaffe *et al.* on the basis of analyticity.

The energy-shift definition of the phase-shift is invariant along the SRG trajectory but for the case of different generators such as those of Wegner and Wilson the behaviour when approaching the infrared limit turns out to be significantly different when bound-states are present. For  $N$ -dimensional hamiltonians the SRG flow has always one unique stable fixed point. In the case of the Wilson generator there are  $N!$  fixed points for non-degenerate hamiltonians but only one is exponentially stable. In the case of the Wegner generator all  $N!$  fixed points are stable. We remind that the SRG evolution with the different generators, while preserving the two-body spectrum, yields asymptotically to infrared fixed-points which only correspond to re-orderings of the eigenvalues and hence contain the same physics of the initial bare two-body Hamiltonian.

With a simple toy model for the nuclear force, we explored the infrared limit of the SRG evolution with both the Wilson and the Wegner generators. While the fixed point is the same for the two generators when no bound-state is supported by the interaction, we have two distinct fixed points when a bound-state is allowed. The evolution with the Wegner generator provides the correct behavior of the interaction in the infrared limit  $\lambda \rightarrow 0$  and defines an ordering of the eigenvalues which can be used to compute the phase-shifts complying to Levinson's theorem without solving the scattering equation. We provide a consistent prescription to shift the eigenvalues in order to obtain the nuclear force in the infrared limit  $\lambda \rightarrow 0$  and also to compute the phase-shifts from the eigenvalues with the correct behavior in both low- and high-momentum regions.

Even though the ordering of states induced by the SRG evolution with the Wegner generator make the phase-shift at low-momentum compliant to Levinson's theorem, there is an optimal ordering which gives the smoothest phase-shifts around the bound-state scale. The optimal ordering corresponds to a shift of the eigenvalues below the bound-state scale while keeping the ascending order above it. The optimal value for the position of the deuteron bound-state, which minimizes the RMS errors, seems to approach the characteristic deuteron momentum scale  $\gamma = 0.23\text{ fm}^{-1}$ . Of course, it must be verified through explicit calculations if this a general result, which holds for any weakly or strongly coupled bound-state.

With the SRG evolution carried out towards  $\lambda \rightarrow 0$ , the difference between the  $^1S_0$  and  $^3S_1$  channels due to the Deuteron bound-state can be seen very clearly. The infrared limit of the SRG evolution with the Wilson generator actually corresponds to an ascending order for the eigenvalues of the interaction, while the Wegner generator preserves the ascending order only above the bound-state scale.

We have also analyzed the  $A = 3$  and  $A = 4$  systems within a simple harmonic oscillator scheme where the main differences between different generators may be clearly appreciated as the critical scale is approached. There appear two branches  $E_\alpha = 4E_t - 3E_d$  and  $E_\alpha = 2E_t$  and the system takes the lowest energy at any rate among all possible states contained in the trial wave function. Our results generate a Tjon-line which matches the expression  $E_\alpha = 4E_t - 3E_d$  found by invoking three-body forces in our previous work for the SRG cutoff below  $\lambda \sim 1\text{fm}^{-1}$  (the factor 4 corresponds to 4 triplets) [25]. We remind that this is the regime which so far remained inaccessible for realistic interactions. The accuracy of the Tjon formula is rather satisfactory and a complementary investigation going beyond the simple variational ansatz and including specifically many-body forces would be most illuminating. The application of the on-shell interactions to few-nucleon systems, light nuclei and nuclear many-body problems (neutron and nuclear matter) for realistic interactions is beyond the scope of this work but is certainly an interesting study we will pursue in forthcoming works on the light of the present findings.

### Acknowledgements

E.R.A. would like to thank the Spanish Mineco (Grant FIS2014-59386-P) and Junta de Andalucía (grant FQM225). S.S. and V.S.T. are supported by FAPESP (grant 2014/04975-9). V.S.T. also thanks FAEPEX (grant 1165/2014) and CNPq (grant 310980/2012-7) for financial support.

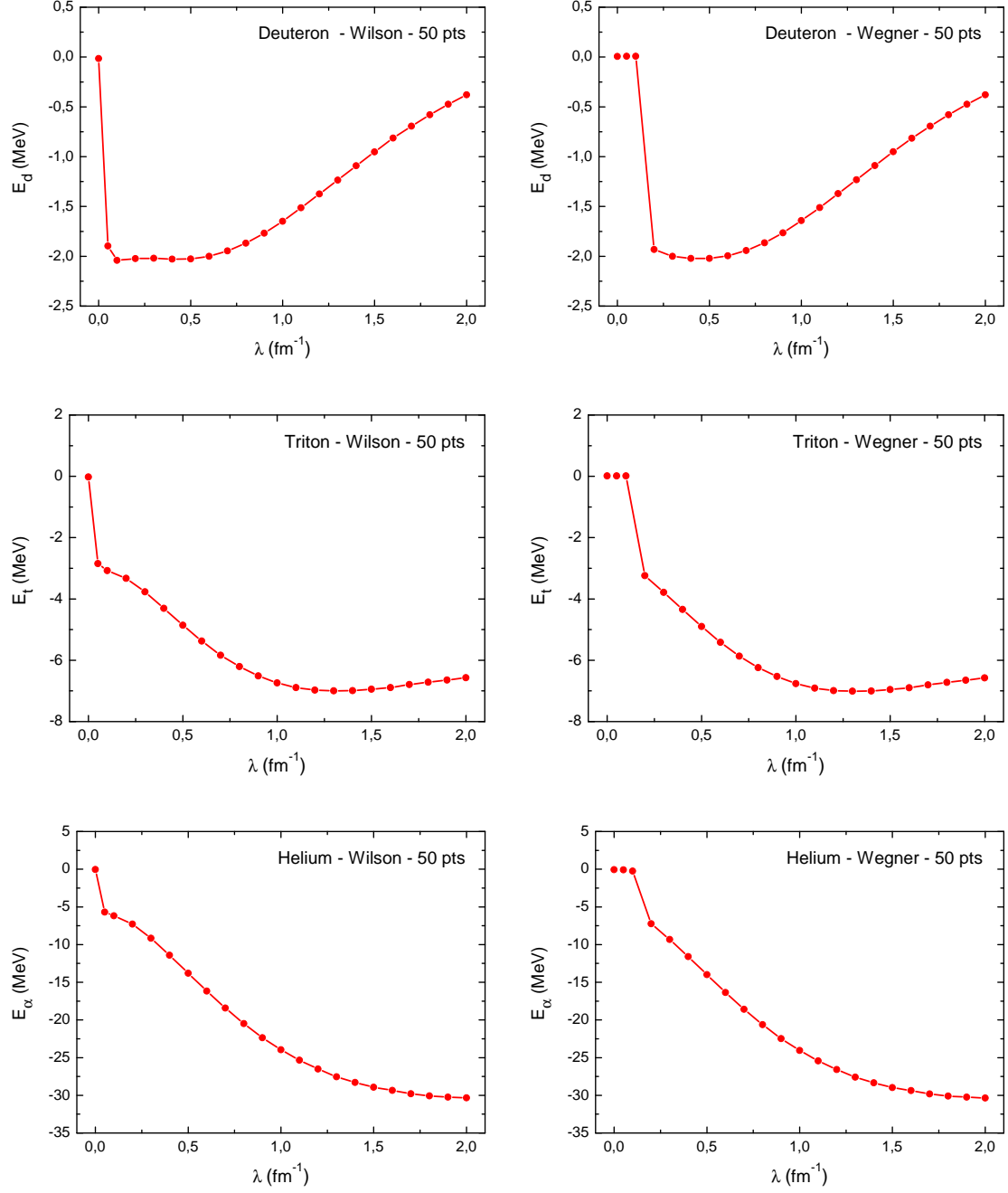


Figure 16: Shell-model variational energies for Deuteron, Triton and Helium obtained from the toy-model separable gaussian potentials ( $\Lambda = 2 \text{ fm}^{-1}$  and  $N = 50$ ) evolved through the SRG transformation using the Wilson and the Wegner generators as a function of the SRG cutoff  $\lambda$ .

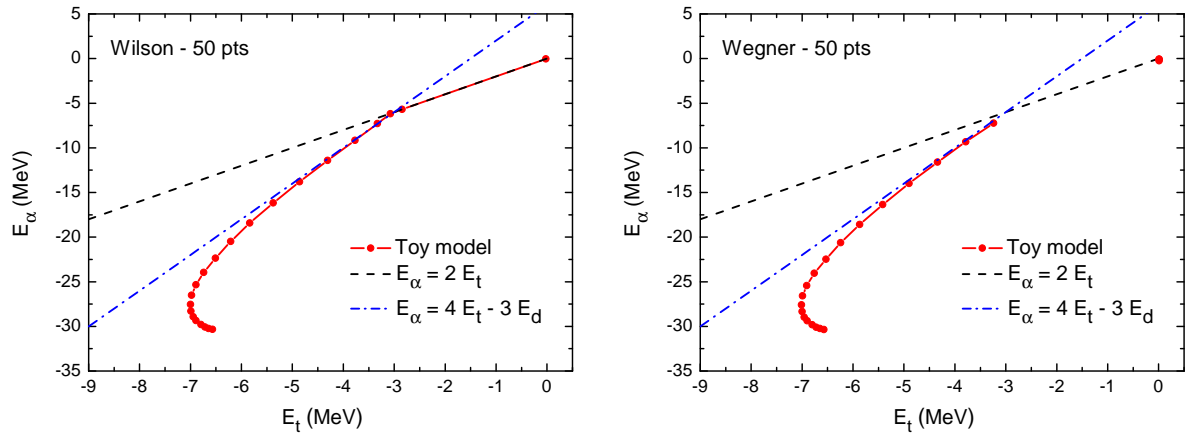


Figure 17: Tjon-lines obtained from the toy-model separable gaussian potentials ( $\Lambda = 2 \text{ fm}^{-1}$  and  $N = 50$ ) evolved through the SRG transformation using the Wilson and the Wegner generators. We compare with the asymptotic lines  $E_\alpha = 4E_t - 3E_d$  and  $E_\alpha = 2E_t$ .

## References

## References

- [1] S. D. Glazek, K. G. Wilson, Renormalization of Hamiltonians, *Phys. Rev. D* **48** (1993) 5863–5872. doi:10.1103/PhysRevD.48.5863.
- [2] S. D. Glazek, K. G. Wilson, Perturbative renormalization group for Hamiltonians, *Phys. Rev. D* **49** (1994) 4214–4218. doi:10.1103/PhysRevD.49.4214.
- [3] F. Wegner, Flow-equations for Hamiltonians, *Annalen der physik* **506** (2) (1994) 77–91.
- [4] S. Kehrein, *The flow equation approach to many-particle systems*, Springer, 2006.
- [5] S. K. Bogner, R. J. Furnstahl, R. J. Perry, Similarity Renormalization Group for Nucleon-Nucleon Interactions, *Phys. Rev. C* **75** (2007) 061001. arXiv:nucl-th/0611045, doi:10.1103/PhysRevC.75.061001.
- [6] S. K. Bogner, R. J. Furnstahl, A. Schwenk, From low-momentum interactions to nuclear structure, *Prog. Part. Nucl. Phys.* **65** (2010) 94–147. arXiv:0912.3688, doi:10.1016/j.ppnp.2010.03.001.
- [7] R. Furnstahl, The Renormalization Group in Nuclear Physics, *Nucl.Phys.Proc.Suppl.* **228** (2012) 139–175. arXiv:1203.1779, doi:10.1016/j.nuclphysbps.2012.06.005.
- [8] R. Furnstahl, K. Hebeler, New applications of renormalization group methods in nuclear physics, *Rept.Prog.Phys.* **76** (2013) 126301. arXiv:1305.3800, doi:10.1088/0034-4885/76/12/126301.
- [9] R. B. Wiringa, V. Stoks, R. Schiavilla, An Accurate nucleon-nucleon potential with charge independence breaking, *Phys.Rev. C* **51** (1995) 38–51. arXiv:nucl-th/9408016, doi:10.1103/PhysRevC.51.38.
- [10] V. G. J. Stoks, R. A. M. Klomp, C. P. F. Terheggen, J. J. de Swart, Construction of high quality N N potential models, *Phys. Rev. C* **49** (1994) 2950–2962. arXiv:nucl-th/9406039, doi:10.1103/PhysRevC.49.2950.
- [11] D. R. Entem, R. Machleidt, Accurate Charge-Dependent Nucleon-Nucleon Potential at Fourth Order of Chiral Perturbation Theory, *Phys. Rev. C* **68** (2003) 041001. arXiv:nucl-th/0304018, doi:10.1103/PhysRevC.68.041001.
- [12] E. Epelbaum, W. Glockle, U.-G. Meissner, The Two-nucleon system at next-to-next-to-next-to-leading order, *Nucl.Phys. A* **747** (2005) 362–424. arXiv:nucl-th/0405048, doi:10.1016/j.nuclphysa.2004.09.107.
- [13] E. D. Jurgenson, P. Navratil and R. J. Furnstahl, Evolution of Nuclear Many-Body Forces with the Similarity Renormalization Group, *Phys. Rev. Lett.* **103**, 082501 (2009) doi:10.1103/PhysRevLett.103.082501 [arXiv:0905.1873 [nucl-th]].
- [14] K. Hebeler, Momentum space evolution of chiral three-nucleon forces, *Phys. Rev. C* **85**, 021002 (2012) doi:10.1103/PhysRevC.85.021002 [arXiv:1201.0169 [nucl-th]].
- [15] K. A. Wendt, Similarity Renormalization Group Evolution of Three-Nucleon Forces in a Hyperspherical Momentum Representation, *Phys.Rev. C* **87** (6) (2013) 061001. arXiv:1304.1431, doi:10.1103/PhysRevC.87.061001.
- [16] T. Frederico, V. Timoteo, L. Tomio, Renormalization of the one pion exchange interaction, *Nucl.Phys. A* **653** (1999) 209–221. arXiv:nucl-th/9902052, doi:10.1016/S0375-9474(99)00234-1.
- [17] V. Timoteo, T. Frederico, A. Delfino, L. Tomio, Recursive renormalization of the singlet one-pion-exchange plus point-like interactions, *Phys.Lett. B* **621** (2005) 109–118. arXiv:nucl-th/0508006, doi:10.1016/j.physletb.2005.06.044.
- [18] V. Timoteo, T. Frederico, A. Delfino, L. Tomio, Nucleon-nucleon scattering within a multiple subtractive renormalization approach, *Phys.Rev. C* **83** (2011) 064005. arXiv:1006.1942, doi:10.1103/PhysRevC.83.064005.
- [19] S. Szpigel, V. S. Timoteo, Power counting and renormalization group invariance in the subtracted kernel method for the two-nucleon system, *J.Phys. G* **39** (2012) 105102. arXiv:1112.5972, doi:10.1088/0954-3899/39/10/105102.
- [20] S. Szpigel, V. S. Timoteo, F. d. O. Duraes, Similarity Renormalization Group Evolution of Chiral Effective Nucleon-Nucleon Potentials in the Subtracted Kernel Method Approach, *Annals Phys.* **326** (2011) 364–405. arXiv:1003.4663, doi:10.1016/j.aop.2010.11.007.
- [21] E. Ruiz Arriola, V. Timoteo, S. Szpigel, Nuclear Symmetries of the similarity renormalization group for nuclear forces, *PoS CD12* (2013) 106. arXiv:1302.3978.
- [22] V. Timoteo, S. Szpigel, E. Ruiz Arriola, Symmetries of the Similarity Renormalization Group for Nuclear Forces, *Phys.Rev. C* **86** (2012) 034002. arXiv:1108.1162, doi:10.1103/PhysRevC.86.034002.
- [23] E. Ruiz Arriola, S. Szpigel, V. Timoteo, The infrared limit of the Similarity Renormalization Group evolution and Levinson’s theorem, *Phys.Lett. B* **735** (2014) 149–156. arXiv:1404.4940, doi:10.1016/j.physletb.2014.06.032.
- [24] Z.-Q. Ma, The Levinson theorem, *J.Phys. A* **39** (2006) R625–R659. doi:10.1088/0305-4470/39/48/R01.
- [25] E. Ruiz Arriola, S. Szpigel, V. Timoteo, Fixed points of the Similarity Renormalization Group and the Nuclear Many-Body Problem, *Few Body Syst.* **55** (2014) 971–975. arXiv:1310.8246, doi:10.1007/s00601-014-0858-7.
- [26] A. Delfino, T. Frederico, V. S. Timoteo, L. Tomio, The Few scales of nuclei and nuclear matter, *Phys. Lett. B* **634** (2006) 185. arXiv:0704.0481, doi:10.1016/j.physletb.2006.01.046.
- [27] H.-W. Hammer, A. Nogga, A. Schwenk, Three-body forces: From cold atoms to nuclei, *Rev. Mod. Phys.* **85** (2013) 197. arXiv:1210.4273, doi:10.1103/RevModPhys.85.197.
- [28] E. Ruiz Arriola, S. Szpigel, V. S. Timoteo, Unitary neutron matter in the on-shell limit arXiv:1412.2077.
- [29] E. Ruiz Arriola, S. Szpigel, V. S. Timoteo, The BCS pairing gap in the on-shell limit of the Similarity Renormalization Group arXiv:1507.02475.
- [30] E. Anderson, et al., Block Diagonalization using SRG Flow Equations, *Phys. Rev. C* **77** (2008) 037001. arXiv:0801.1098, doi:10.1103/PhysRevC.77.037001.
- [31] E. Ruiz Arriola, S. Szpigel, V. S. Timoteo, Implicit Versus Explicit Renormalization of the NN Force: An S-Wave Toy Model, *Few Body Syst.* **55** (2014) 989–992. arXiv:1310.8526, doi:10.1007/s00601-014-0811-9.
- [32] E. Ruiz Arriola, S. Szpigel, V. Timoteo, Implicit vs Explicit Renormalization and Effective Interactions, *Phys.Lett. B* **728** (2014) 596–601. arXiv:1307.1231, doi:10.1016/j.physletb.2013.12.038.
- [33] V. I. Kukulin, V. N. Pomerantsev, O. A. Rubtsova, Discrete representation of the spectral shift function and the multichannel s-matrix, *JETP letters* **90** (5) (2009) 402.

- [34] O. Rubtsova, V. Kukulin, V. Pomerantsev, A. Faessler, New approach toward a direct evaluation of the multichannel multienergy S matrix without solving the scattering equations, *Phys.Rev. C* 81 (2010) 064003. doi:10.1103/PhysRevC.81.064003.
- [35] V. Pomerantsev, V. Kukulin, O. Rubtsova, New general approach in few-body scattering calculations: Solving discretized Faddeev equations on a graphics processing unit, *Phys.Rev. C* 89 (6) (2014) 064008. arXiv:1404.5253, doi:10.1103/PhysRevC.89.064008.
- [36] O. A. Rubtsova, V. I. Kukulin, V. N. Pomerantsev, Wave-packet continuum discretization for quantum scattering, *Annals Phys.* 360 (2015) 613–654. arXiv:1501.02531, doi:10.1016/j.aop.2015.04.028.
- [37] N. Graham, R. Jaffe, M. Quandt, H. Weigel, Finite energy sum rules in potential scattering, *Annals Phys.* 293 (2001) 240. arXiv:quant-ph/0104136, doi:10.1006/aphy.2001.6173.
- [38] V. S. Timoteo, S. Szpigel, E. R. Arriola, Symmetries of the Similarity Renormalization Group for Nuclear Forces, *Phys.Rev. C* 86 (2012) 034002. arXiv:1108.1162, doi:10.1103/PhysRevC.86.034002.
- [39] B. Dainton, R. Furnstahl, R. Perry, Universality in Similarity Renormalization Group Evolved Potential Matrix Elements and T-Matrix Equivalence, *Phys.Rev. C* 89 (2014) 014001. arXiv:1310.6690, doi:10.1103/PhysRevC.89.014001.
- [40] E. D. Jurgenson, Applications of the Similarity Renormalization Group to the Nuclear Interaction, PhD Thesis arXiv:0912.2937.
- [41] S. K. Bogner, T. T. S. Kuo, A. Schwenk, D. R. Entem, R. Machleidt, Towards a unique low momentum nucleon nucleon interaction, *Phys. Lett. B* 576 (2003) 265–272. arXiv:nuc1-th/0108041, doi:10.1016/j.physletb.2003.10.012.
- [42] W. Li, E. Anderson, R. Furnstahl, The Similarity Renormalization Group with Novel Generators, *Phys.Rev. C* 84 (2011) 054002. arXiv:1106.2835, doi:10.1103/PhysRevC.84.054002.
- [43] N. M. Dicaire, C. Omand, P. Navratil, Alternative similarity renormalization group generators in nuclear structure calculations, *Phys.Rev. C* 90 (3) (2014) 034302. arXiv:1406.1815, doi:10.1103/PhysRevC.90.034302.
- [44] S. Szpigel, V. S. Timoteo, F. O. Duraes, Similarity Renormalization Group Evolution of Chiral Effective Nucleon-Nucleon Potentials in the Subtracted Kernel Method Approach, *Annals Phys.* 326 (2011) 364. arXiv:1003.4663, doi:10.1016/j.aop.2010.11.007.
- [45] S. Szpigel, R. J. Perry, Simple applications of effective field theory and similarity renormalization group methods arXiv:nuc1-th/9906031.
- [46] B. D. Jones, R. J. Perry, Similarity flow of a neutral scalar coupled to a fixed source, arXiv:nuc1-th/1305.6599 arXiv:1305.6599.
- [47] A. N. Kolmogorov, S. Fomin, Elements of the theory of functions and functional analysis, Vol. 1, Courier Corporation, 1999.
- [48] S. Weinberg, Quasiparticles and the Born Series, *Phys.Rev.* 131 (1963) 440–460. doi:10.1103/PhysRev.131.440.
- [49] S. Bogner, R. Furnstahl, S. Ramanan, A. Schwenk, Convergence of the Born series with low-momentum interactions, *Nucl.Phys. A* 773 (2006) 203–220. arXiv:nuc1-th/0602060, doi:10.1016/j.nuclphysa.2006.05.004.
- [50] R. Navarro Pérez, J. Amaro, E. Ruiz Arriola, Low energy chiral two pion exchange potential with statistical uncertainties, *Phys.Rev. C* 91 (5) (2015) 054002. arXiv:1411.1212, doi:10.1103/PhysRevC.91.054002.
- [51] B. P. Demidovich, I. A. Maron, G. Yankovsky, Computational mathematics, Mir publishers Moscow, 1973.
- [52] R. W. Brockett, Dynamical Systems That Sort Lists, Diagonalize Matrices and Solve Linear Programming Problems, *Linear Algebra and Its Applications* 146 (1991) 79–91.
- [53] J. V. Steele, R. Furnstahl, Regularization methods for nucleon-nucleon effective field theory, *Nucl.Phys. A* 637 (1998) 46–62. arXiv:nuc1-th/9802069, doi:10.1016/S0375-9474(98)00219-X.
- [54] V. G. J. Stoks, R. A. M. Kompl, M. C. M. Rentmeester, J. J. de Swart, Partial wave analysis of all nucleon-nucleon scattering data below 350-MeV, *Phys. Rev. C* 48 (1993) 792–815. doi:10.1103/PhysRevC.48.792.
- [55] R. Navarro Pérez, J. Amaro, E. Ruiz Arriola, Partial Wave Analysis of Nucleon-Nucleon Scattering below pion production threshold, *Phys.Rev. C* 88 (6) (2013) 024002. arXiv:1304.0895, doi:10.1103/PhysRevC.88.024002, 10.1103/PhysRevC.88.069902.
- [56] R. Navarro Pérez, J. Amaro, E. Ruiz Arriola, Coarse-grained potential analysis of neutron-proton and proton-proton scattering below the pion production threshold, *Phys.Rev. C* 88 (6) (2013) 064002. arXiv:1310.2536, doi:10.1103/PhysRevC.88.064002.
- [57] R. N. Perez, J. Amaro, E. R. Arriola, Coarse grained NN potential with Chiral Two Pion Exchange, *Phys.Rev. C* 89 (2014) 024004. arXiv:1310.6972, doi:10.1103/PhysRevC.89.024004.
- [58] R. Navarro Perez, J. Amaro, E. Ruiz Arriola, Statistical Error analysis of Nucleon-Nucleon phenomenological potentials, *Phys.Rev. C* 89 (2014) 064006. arXiv:1404.0314, doi:10.1103/PhysRevC.89.064006.
- [59] S. D. Glazek, R. J. Perry, The impact of bound states on similarity renormalization group transformations, *Phys. Rev. D* 78 (2008) 045011. arXiv:0803.2911, doi:10.1103/PhysRevD.78.045011.
- [60] K. A. Wendt, R. J. Furnstahl, R. J. Perry, Decoupling of Spurious Deep Bound States with the Similarity Renormalization Group, *Phys. Rev. C* 83 (2011) 034005. arXiv:1101.2690, doi:10.1103/PhysRevC.83.034005.
- [61] E. Ruiz Arriola, S. Szpigel, V. Timteo, Implicit and explicit renormalization: two complementary views of effective interactions, *Annals Phys.* 353 (2014) 129–149. arXiv:1407.8449, doi:10.1016/j.aop.2014.11.010.
- [62] B. S. DeWitt, Transition from discrete to continuous spectra, *Phys.Rev.* 103 (1956) 1565–1571. doi:10.1103/PhysRev.103.1565.
- [63] N. Fukuda, R. Newton, Energy Level Shifts in a Large Enclosure, *Phys.Rev.* 103 (1956) 1558–1564. doi:10.1103/PhysRev.103.1558.
- [64] G. Parisi, Statistical field theory, Addison-Wesley, 1988.
- [65] J. Muga, R. Levine, Stationary scattering theories, *Physica Scripta* 40 (2) (1989) 129.
- [66] L. D. Landau, E. M. Lifshitz, Quantum mechanics: non-relativistic theory, Vol. 3, Elsevier, 2013.